

# We are IntechOpen, the world's leading publisher of Open Access books Built by scientists, for scientists

6,900

Open access books available

186,000

International authors and editors

200M

Downloads

Our authors are among the

154

Countries delivered to

TOP 1%

most cited scientists

12.2%

Contributors from top 500 universities



WEB OF SCIENCE™

Selection of our books indexed in the Book Citation Index  
in Web of Science™ Core Collection (BKCI)

Interested in publishing with us?  
Contact [book.department@intechopen.com](mailto:book.department@intechopen.com)

Numbers displayed above are based on latest data collected.  
For more information visit [www.intechopen.com](http://www.intechopen.com)



# Micromechanical Failure Analysis of Unidirectional Composites

*Zheng-Ming Huang*

## Abstract

Internal stresses in the fiber and matrix of a unidirectional (UD) composite obtained by any micromechanics model are homogenized quantities. They must be converted into true values before an effective specifically failure and strength property of the composite can be predicted in terms of the fiber and matrix properties only. As elastic property of a material does not depend on the magnitude of its stresses, the predictions of an elastic property of the composite based on the homogenized and true stresses of the constituents are the same, concealing the fact that the elastic property should be predicted based on the true stresses as well. The conversion of all of the internal stress components has been shown in this chapter. Predictability of a total number of 12 micromechanics models for the stiffness and strength of a UD composite is assessed against the experimental data of the 9 UD composites provided in three worldwide failure exercises (WWFEs). Bridging Model exhibits overall the best accuracy in both the stiffness and the strength predictions. Further, the smallest fiber volume in a RVE (representative volume element) for an FE (finite element) approach plays a much more dominant role than other issues such as a random fiber arrangement pattern to achieve the highest simulation accuracy. Finally, consistency of a micromechanics model in calculating the internal stresses of a composite is an issue that should be taken into account. Only Bridging Model is consistent. A non-consistency implies that a full three-dimensional (3D) model should be used to predict an effective property, e.g., failure behavior of a composite even though it is only subjected to a uniaxial load, and a 3D RVE geometry should be discretized if a numerical micromechanics approach is applied.

**Keywords:** composites, micromechanics, stress concentration factors, interface crack, failure analysis, strength prediction, consistency, fiber arrangement arrays

## 1. Introduction

Fiber-reinforced composites have been used as a primary-load carrying structural material in many engineering areas especially in aerospace industry. Due to their anisotropy, the mechanical properties of the composites are difficult or expensive to understand through experiments. Establishment of mathematical models to link the overall behaviors of the composites with their constituent structures and properties is an objective of micromechanics. As any continuous fiber-reinforced composite structure can be subdivided into a combination of a

series of unit cells or RVEs [1], which can be considered as UD composites in their local coordinate system, a micromechanics analysis of a UD composite is fundamental.

So far, numerous micromechanical models have been developed to predict elastic properties of the composites from those of the constituent fiber and matrix materials [2–4]. On the other hand, very few of them have been applied to estimate failure and strength behaviors of the composites only based on the original constituent data measured independently with a reasonable accuracy [5]. This is attributed to that the internal stresses in the fiber and matrix of a composite obtained by a micromechanics theory are homogeneous quantities. They must be converted into true values before an effective property of the composite is predicted in terms of the original constituent properties. An elastic property (modulus, stiffness, etc.) of a material does not depend on the magnitude of the stresses in it, as long as they do not exceed the elastic limit of the material. Hence, the predictions of an elastic property of the composite based on the homogenized and true stresses of the constituents are the same, concealing the fact that the composite elastic property should also be predicted based on the true stresses. The stress field of the fiber is uniform [6, 7]. Its homogenized and true stresses are the same. A true stress of the matrix is obtained by multiplying its homogeneous counterpart with a stress concentration factor (SCF) of the matrix in the composite. This is because a plate with a hole generates a stress concentration if subjected to an in-plane tension. When the hole is filled with a fiber of different properties, a stress concentration occurs as well.

The most significant feature is that such an SCF cannot be defined, following a classical approach, as a maximum point-wise stress divided by the overall applied one. Otherwise, the resulting SCF would be infinite if there is an interface crack or debonding on a fiber and matrix interface, since at the crack tip, a matrix stress is singular. All of the SCFs of the matrix in a composite have been obtained [8–11] and are summarized in this chapter.

Another objective of this chapter is to make a critical assessment for the predicability of 12 well-known micromechanical models for the stiffness and mainly failure and strength of a UD composite, based on the original fiber and matrix properties and the fiber volume fraction. By “original,” it is meant that the properties are either measured independently using monolithic material, e.g., matrix specimens or documented in a recognized material database. The previous comparisons, e.g., Refs. [12–14], were made essentially for the stiffness predictions by different models. Seldom have been found for the strength predictions. The models considered in this chapter are Eshelby’s method [6, 15], Bridging Model [16], Mori-Tanaka method [17, 18], rule of mixture method [19], Chamis model [20], modified rule of mixture method [19], Halpin-Tsai formulae [21], Hill-Hashin-Christensen-Lo model [22], self-consistent method [15], generalized self-consistent method [15, 23], double inclusion method [4], and finite element method (FEM) [24] with different fiber arrangement patterns in a unit cell or RVE. The measured stiffness and strength data of all of the nine independent UD composites adopted in three WWFEs [25–27] are used as benchmark to judge the prediction accuracy of each model. An accuracy ranking is made based on the overall correlation errors between the models’ predictions and the experiments.

Numerical micromechanics such as FE approaches are popular in the current literature. What kind of fiber arrangement pattern should be chosen in a RVE? By definition, the RVE geometry, on which a homogenization is made, should be infinitesimal. In reality, however, a finite volume for a RVE has to be used. Thus, various choices exist. Many people [28–30] deemed that a random arrangement pattern with quite a number of fibers, e.g., 30 [31], 40 [32], or even 120 [33], should

be contained in the RVE. It is shown among the four different patterns considered in this chapter the one with the smallest fiber volume results in the highest prediction accuracy.

Finally, consistency in the internal stress calculation deserves an attention. Any micromechanics model can result in two sets of formulae, i.e., two-dimensional (2D) and three-dimensional (3D) formulae, for homogenized internal stresses in the fiber and matrix of a composite. When the composite is subjected to a planar load, either the 2D or the 3D formulae can be applied to calculate the internal stresses. If the stress components in the fiber and matrix by the 2D and the 3D formulae are exactly the same, the model is said to be consistent in the internal stress calculation. It is shown in the chapter that among the 12 theories considered, only Bridging Model is consistent. Thus, if any other models specifically the numerical micromechanics method is applied to determine the internal stresses, its full 3D formulae should be made in use, even though the composite is subjected to only a uniaxial load.

In short, the topics addressed in this chapter are important to the micromechanical analysis of an effective mechanical property of a composite. If one would like to estimate its failure and strength behavior under an arbitrary load condition only from its constituent information, the true stress theory as described in this chapter is inevitable.

## 2. Fundamental for internal stresses

A composite is heterogenous by nature. Any stress and strain should be defined upon averaged quantities with respect to its RVE of a volume  $V'$  through.

$$\sigma_i = \left( \int_{V'} \tilde{\sigma}_i dV \right) / V' = V_f \sigma_i^f + V_m \sigma_i^m, \quad (1)$$

$$\varepsilon_i = \left( \int_{V'} \tilde{\varepsilon}_i dV \right) / V' = V_f \varepsilon_i^f + V_m \varepsilon_i^m. \quad (2)$$

It must be realized that by definition  $V'$  should be infinitesimal, and a resulting stress or strain, with  $\sim$  on head, represents a point-wise quantity. If  $V'$  is finite, the corresponding one is called a homogenized quantity. In Eqs. (1) and (2),  $V$  is a volume fraction with  $V_f + V_m = 1$ . A super-/subscript  $f$  or  $m$  refers to the fiber or matrix, whereas a quantity without any suffix is related to the composite.

Using a bridging equation,  $\{\sigma_i^m\} = [A_{ij}] \{\sigma_j^f\}$ , and the constitutive relationships,  $\{\varepsilon_i^f\} = [S_{ij}^f] \{\sigma_j^f\}$ ,  $\{\varepsilon_i^m\} = [S_{ij}^m] \{\sigma_j^m\}$ , and  $\{\varepsilon_i\} = [S_{ij}] \{\sigma_j\}$ , the internal stresses in the fiber and matrix together with the compliance tensor of the composite are found to be [16]

$$\{\sigma_i^f\} = (V_f [I] + V_m [A_{ij}])^{-1} \{\sigma_j\}, \quad (3)$$

$$\{\sigma_i^m\} = [A_{ij}] (V_f [I] + V_m [A_{ij}])^{-1} \{\sigma_j\}. \quad (4)$$

$$[S_{ij}] = \left( V_f [S_{ij}^f] + V_m [S_{ij}^m] [A_{ij}] \right) (V_f [I] + V_m [A_{ij}])^{-1}. \quad (5)$$

$[S_{ij}^f]$  and  $[S_{ij}^m]$  are the compliance tensors of the fiber and matrix, respectively, and  $[I]$  is a unit tensor. From Eq. (5), the bridging tensor is solved as

$$[A_{ij}] = V_f \left( [S_{ij}] - [S_{ij}^m] \right)^{-1} \left( [S_{ij}^f] - [S_{ij}] \right) / V_m. \quad (6)$$

The prediction of elastic moduli is equivalent to the calculation of internal stresses in the fiber and matrix of the same composite.

### 3. Highlight on micromechanics models

A different micromechanics model corresponds to a different bridging tensor. Perhaps the most compact bridging tensor is given by Bridging Model [16], of which the non-zero bridging tensor elements are expressed as follows:

$$a_{11} = E^m / E_{11}^f, \quad (7.1)$$

$$a_{12} = a_{13} = \frac{\nu^m E_{11}^f - E^m \nu_{12}^f}{E^m - E_{11}^f} (a_{11} - a_{22}), \quad (7.2)$$

$$a_{22} = a_{33} = a_{44} = 0.3 + 0.7 \frac{E^m}{E_{22}^f}, \quad (7.3)$$

$$a_{55} = a_{66} = 0.3 + 0.7 \frac{G^m}{G_{12}^f}. \quad (7.4)$$

$E_{11}^f$ ,  $E_{22}^f$ , and  $G_{12}^f$  are longitudinal, transverse, and in-plane shear moduli of the fiber, respectively.  $\nu_{12}^f$  is its longitudinal Poisson's ratio.  $E^m$  and  $G^m$  are Young's and shear moduli of the matrix. Substituting the so-defined bridging tensor into Eqs. (3) and (4) leads to

$$\sigma_{11}^f = \frac{\sigma_{11}^0}{V_f + V_m a_{11}} - \frac{V_m a_{12} (\sigma_{22}^0 + \sigma_{33}^0)}{(V_f + V_m a_{11}) (V_f + V_m a_{22})}, \quad (8.1)$$

$$\sigma_{11}^m = \frac{a_{11} \sigma_{11}^0}{V_f + V_m a_{11}} + \frac{V_f a_{12} (\sigma_{22}^0 + \sigma_{33}^0)}{(V_f + V_m a_{11}) (V_f + V_m a_{22})}, \quad (8.2)$$

$$\sigma_{ij}^f = \frac{\sigma_{ij}^0}{V_f + V_m a_{22}}, \quad ij = 22, 33, \text{ and } 23, \quad (8.3)$$

$$\sigma_{ij}^m = \frac{a_{22} \sigma_{ij}^0}{V_f + V_m a_{22}}, \quad ij = 22, 33, \text{ and } 23, \quad (8.4)$$

$$\sigma_{ij}^f = \frac{\sigma_{ij}^0}{V_f + V_m a_{66}}, \quad ij = 12 \text{ and } 13, \quad (8.5)$$

$$\sigma_{ij}^m = \frac{a_{66} \sigma_{ij}^0}{V_f + V_m a_{66}}, \quad ij = 12 \text{ and } 13, \quad (8.6)$$

$\{\sigma_{11}^0, \sigma_{22}^0, \sigma_{33}^0, \sigma_{23}^0, \sigma_{13}^0, \text{ and } \sigma_{12}^0\}$  are any arbitrary loads applied on the composite.

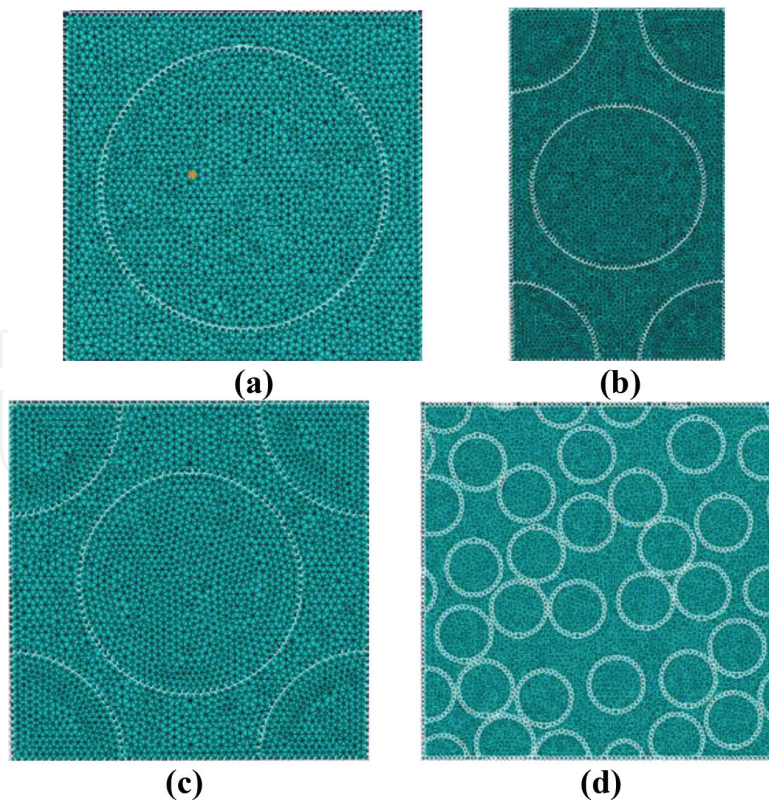


**Figure 1.** Different RVEs for a UD composite used in FE approach: (a) square fiber array, (b) hexagonal fiber array, (c) square-diagonal fiber array, and (d) random fiber array.

The other analytical models are summarized in Appendix A. However, numerical micromechanics methods are even more widely applied in the current literature [34–36]. Among, an FE approach is the most common. In this approach, the fiber and matrix in a RVE geometry are discretized, respectively, into a number of elements with prescribed boundary conditions. After the stresses (i.e., point-wise quantities) in the fiber and matrix of the RVE under any load are obtained through an FE package such as ABAQUS, they are homogenized as per Eq. (1) and the bridging tensor is determined following a method of Ref. [37]. The specification of the boundary conditions has become standard [36]. Thus, different solutions only come from different RVE geometries used.

In this chapter, four kinds of RVE geometries with the same boundary conditions are chosen for the comparison. They are square fiber array [38] (**Figure 1a**), hexagonal array [36] (**Figure 1b**), square-diagonal array [39] (**Figure 1c**), and random array with 30 fibers involved [28, 31] (**Figure 1d**). Our solutions are the same as those in Ref. [36] for **Figure 1b**, in Ref. [39] for **Figure 1c**, and in Ref. [31] for **Figure 1d**, respectively.

#### 4. Assessment on stiffness prediction

Hinton et al. organized three WWFEs to judge efficiency of the current theories for composites [5]. A total number of nine independent material systems were used. Mechanical properties of the fibers and matrices as well as fiber volume fractions of the nine UD composites were provided [25–27] and cited in **Table B.1** (see Appendix B). Measured effective properties of the composites from the exercise organizers [25–27], which are used as a benchmark to assess the predictability of the 12 models, are listed in **Table B.2**. Predictions for the five effective elastic moduli of

Model	N	Averaged error*	Error ratio	Rank	Model	N	Averaged error*	Error ratio	Rank
Bridging model	45	10.38%	1.0	1	Halpin-Tsai formulae	45	19.24%	1.85	9
FE-square	45	13.08%	1.26	2	Modified rule of mixture	45	19.35%	1.86	10
Double inclusion method	45	13.6%	1.31	3	Mori-Tanaka method	45	19.59%	1.89	11
Chamis model	45	14.09%	1.36	4	FE-square diagonal	45	21.48%	2.07	12
Hill-Hashin-C-L model	33	17.22%	1.66	5	Self-consistent method	45	21.82%	2.1	13
FE-random	45	17.57%	1.69	6	Rule of mixture method	45	28.4%	2.74	14
Generalized self-consistent	45	18.14%	1.75	7	Eshelby's method	45	30.72%	2.96	15
FE-hexagonal	45	19.05%	1.84	8					

\* =  $\frac{1}{N} \sum_{i=1}^N \text{abs}(\text{error})_i$ .

**Table 1.**

Overall averaged errors in prediction of the elastic moduli of the nine UD composites by different models.

each of the 9 composites by the 12 models are made and are summarized in **Table B.3**. Relative error of each predicted result in comparison with the measured counterpart (**Table B.2**) is calculated. The overall averaged errors by the 12 models are indicated in **Table 1**, in which FE-square, FE-hexagonal, FE-square-diagonal, and FE-random stand for the FEM solutions based on **Figure 1a–d**, respectively.

It is seen from the table that Bridging Model exhibits overall the highest accuracy in the stiffness prediction, with an overall correlation error of 10.48%. The second smallest error, 13.06%, is achieved by the FE-square array. The FE approach with a random fiber array of 30 fibers results in a correlation error of 17.57%, which is 34.5% less accurate than the FE approach with the square fiber array. The other two fiber arrangement patterns, the hexagonal and the square-diagonal fiber arrays, make the correlation even poorer than the random fiber arrangement. Although the four kinds of fiber arrangement patterns considered in this work may be limited, compared to unlimited possibilities in fiber arrangements, the present study confirms that the minimum fiber volume in the RVE geometry for a composite is the most dominant factor to influence the simulation accuracy, as long as suitable boundary conditions have been equally specified. **Table 1** also indicates that three analytical micromechanics models, Bridging Model, double inclusion method, and Chamis model, possess sufficient accuracy in modeling of composite stiffness.

The largest correlation error, 30.7%, is assumed by Eshelby's method. In addition to it, there are three other models attaining an averaged correlation error of more than 20% in the stiffness prediction. They are the FE-square diagonal fiber array, self-consistent method, and rule of mixture method.

## 5. SCFs of the matrix in a composite

### 5.1 Background

Let the E-glass/LY556 UD composite in **Table B.1** be subjected to only a transverse tension,  $\sigma_{22}^0$ , which will fail from a matrix failure. The only non-zero internal

stresses of the matrix from Eqs. (8.2), (8.4), and (8.6) are  $\sigma_{11}^m = 0.134\sigma_{22}^0$  and  $\sigma_{22}^m = 0.442\sigma_{22}^0$ . Thus, the transverse tensile strength of the composite is  $\sigma_{22}^{u,t} = Y_m/0.422$ , where  $Y_m$  is the in situ transverse tensile strength of the matrix in the composite. Setting  $Y_m = \sigma_{u,t}^m = 80$  MPa (Table B.2), where  $\sigma_{u,t}^m$  is the original tensile strength of the matrix, one obtains  $\sigma_{22}^{u,t} = 181$  MPa, which is more than 5.2 times greater than 35 MPa, the measured counterpart of the composite (Table B.2). A similar conclusion can be drawn no matter which other composite is considered or another micromechanics theory is employed. This implies that the homogenized internal stresses evaluated through Eqs. (3) and (4) must be converted into “true” values before a failure assessment can be made against the original strength data of the constituents. As point-wise strains in the fiber are uniform [6], its homogenized and true stresses are the same. However, those in the matrix are not. Each of its true stresses is obtained by multiplying the homogenized counterpart with a factor, which is agreed to call an SCF of the matrix in the composite.

## 5.2 Definition

The most significant feature, as aforementioned, is that such an SCF is no longer obtainable from a classical approach. Thus, the new definition must be made on an averaged stress. But with respect to which kind of geometry the averaging should be performed? A classical SCF was obtained by a point-wise (something like zero-dimensional) stress divided by an overall applied one, which is in fact a 2D quantity averaged with respect to the boundary surface. By similarity, a present SCF must be defined as a line-averaged (one-dimensional) stress of the matrix divided by a volume-averaged (3D) one since three is the maximum attainable dimension in the denominator. An SCF of the matrix subjected to a transverse load is derived through [10]

$$K_{22}(\varphi) = \frac{1}{\left| \begin{matrix} \vec{R}_\varphi^b \\ \vec{R}_\varphi^a \end{matrix} \right|} \int \frac{\tilde{\sigma}_{22}^m}{(\sigma_{22}^m)_{BM}} d|\vec{R}_\varphi|, \quad (9)$$

in which  $\tilde{\sigma}_{22}^m$  is a point-wise stress of the matrix determined on a concentric cylinder assemblage (CCA) model along the loading direction;  $(\sigma_{22}^m)_{BM}$  is given by Bridging Model, i.e., by Eq. (8.4),  $\varphi$  is the inclined angle of the outward normal to a failure surface under the given load, and  $\vec{R}_\varphi^a$  and  $\vec{R}_\varphi^b$  are the vectors of  $\vec{R}_\varphi$  at the surfaces of the fiber and matrix cylinders within the RVE, respectively, where  $b = a/\sqrt{V_f}$ .

## 5.3 Transverse SCFs

In such a load case, the explicit integration of Eq. (9) leads to [8–10]

$$K_{22}(\varphi) = \left\{ 1 + \frac{A}{2} \sqrt{V_f} \cos 2\varphi + \frac{B}{2(1 - \sqrt{V_f})} \left[ V_f^2 \cos 4\varphi + 4V_f \cos^2 \varphi (1 - 2 \cos 2\varphi) + \sqrt{V_f} (2 \cos 2\varphi + \cos 4\varphi) \right] \right\} (V_f + a_{22}V_m)/a_{22}, \quad (10.1)$$

$$A = \frac{2E_{22}^f E^m (\nu_{12}^f)^2 + E_{11}^f \{E^m (\nu_{23}^f - 1) - E_{22}^f [2(\nu^m)^2 + \nu^m - 1]\}}{E_{11}^f [E_{22}^f + E^m (1 - \nu_{23}^f) + E_{22}^f \nu^m] - 2E_{22}^f E^m (\nu_{12}^f)^2}, \quad (10.2)$$

$$B = \frac{E^m (1 + \nu_{23}^f) - E_{22}^f (1 + \nu^m)}{E_{22}^f [\nu^m + 4(\nu^m)^2 - 3] - E^m (1 + \nu_{23}^f)}. \quad (10.3)$$

Under a transverse tension, the failure surface of the composite is perpendicular to the loading and hence  $\varphi = 0$  (**Figure 2a**). When a transverse compression is applied, the failure surface of the composite has an inclined angle with the loading [31]. The inclined angle,  $\varphi = \phi$  (**Figure 2b**), between the outward normal to the failure surface and the loading, can be determined by virtue of Mohr's theory as [9]

$$\phi = \frac{\pi}{4} + \frac{1}{2} \arcsin \frac{\sigma_{u,c}^m - \sigma_{u,t}^m}{2\sigma_{u,c}^m}. \quad (11)$$

The transverse tensile, transverse compressive, and transverse shear SCFs of the matrix in the composite are given as [9–11]

$$K_{22}^t = K_{22}(0), \quad (12.1)$$

$$K_{22}^c = K_{22}(\phi), \quad (12.2)$$

$$K_{23} = 2\sigma_{u,s}^m \sqrt{\frac{K_{22}^t K_{22}^c}{\sigma_{u,t}^m \sigma_{u,c}^m}}, \quad (12.3)$$

$\sigma_{u,t}^m$ ,  $\sigma_{u,c}^m$ , and  $\sigma_{u,s}^m$  are the original tensile, compressive, and shear strengths of the matrix, respectively.

#### 5.4 SCF under longitudinal shear

A longitudinal shear SCF of the matrix is given by [11]

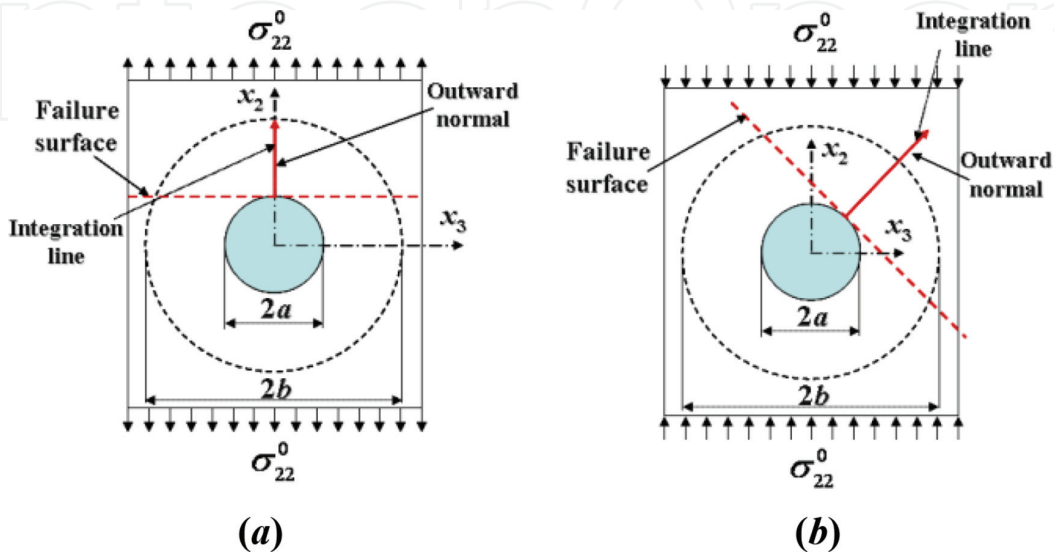


**Figure 2.** Schematic of a RVE used in defining SCF of matrix in a composite subjected to (a) a transverse tension and (b) a transverse compression.

$$K_{12} = \frac{\left[ 1 - V_f \frac{G_{12}^f - G^m}{G_{12}^f + G^m} \left\{ \pi \sqrt{V_f} \left[ \frac{1}{4V_f} - \frac{4}{128} - \frac{2}{512} V_f - \frac{5}{4096} V_f^2 \right] - \frac{1}{3} \right\} \right]}{(V_f + a_{66} V_m)}, \quad (13)$$

### 5.5 SCFs under equally biaxial transverse loads

Eq. (9) designates a general rule to determine any SCF of the matrix in the composite. Under an equally biaxial transverse tension or compression (**Figure 3**), a point-wise stress of the matrix in the  $x_2$ -direction is obtained through a coordinate transformation:

$$\begin{aligned} \tilde{\sigma}_{22}^m = & \left[ \tilde{\sigma}_{\rho\rho}^m(\sigma_{22}^0) + \tilde{\sigma}_{\rho\rho}^m(\sigma_{33}^0) \right] \cos^2 \varphi + \left[ \tilde{\sigma}_{\varphi\varphi}^m(\sigma_{22}^0) + \tilde{\sigma}_{\varphi\varphi}^m(\sigma_{33}^0) \right] \sin^2 \varphi \\ & - \left[ \tilde{\sigma}_{\rho\varphi}^m(\sigma_{22}^0) + \tilde{\sigma}_{\rho\varphi}^m(\sigma_{33}^0) \right] \sin 2\varphi, \end{aligned} \quad (14)$$

where [41]

$$\tilde{\sigma}_{\rho\rho}^m(\sigma_{22}^0) = \frac{\sigma_{22}^0}{2} \left\{ 1 + Aa^2\rho^{-2} + [1 + B(4a^2\rho^{-2} - 3a^4\rho^{-4})] \cos 2\varphi \right\}, \quad (15.1)$$

$$\tilde{\sigma}_{\varphi\varphi}^m(\sigma_{22}^0) = \frac{\sigma_{22}^0}{2} \left[ 1 - Aa^2\rho^{-2} - (1 - 3Ba^4\rho^{-4}) \cos 2\varphi \right], \quad (15.2)$$

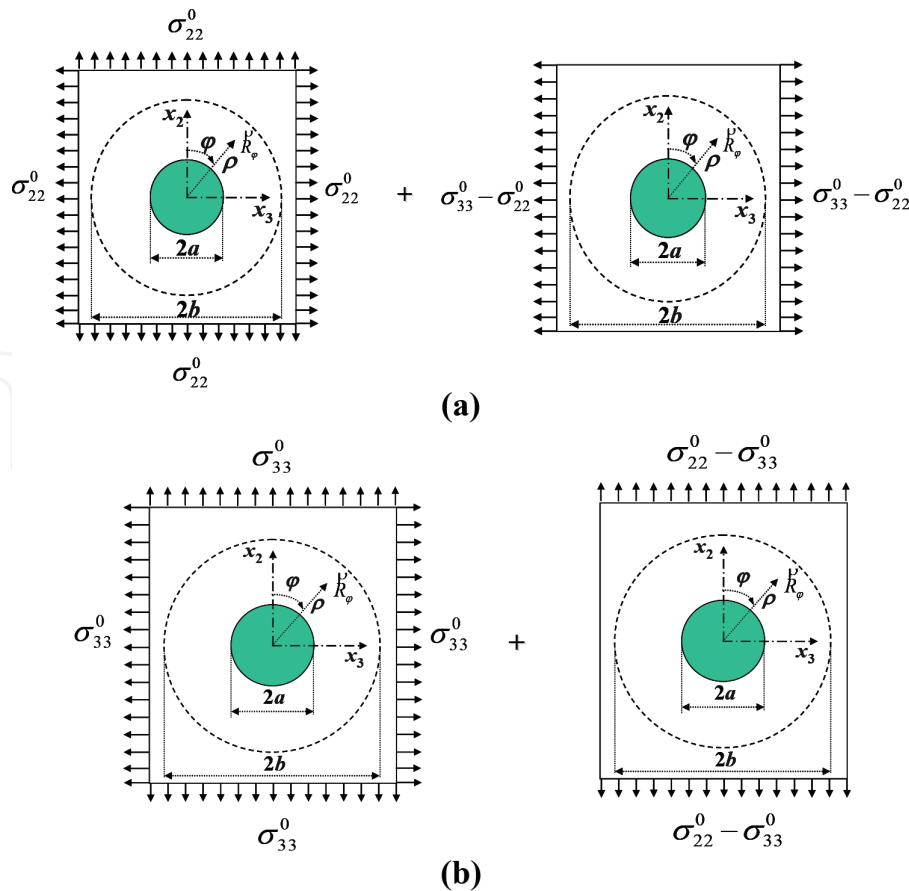


**Figure 3.** Any biaxially transverse loads can be separated into superposition of an equally biaxial load and a uniaxial transverse tension either along  $x_3$ -direction (a), if  $\sigma_{33}^0 - \sigma_{22}^0 > 0$ , or along  $x_2$ -direction (b), if  $\sigma_{22}^0 - \sigma_{33}^0 > 0$ .

$$\tilde{\sigma}_{\rho\varphi}^m(\sigma_{22}^0) = -\frac{\sigma_{22}^0}{2} [1 - B(2a^2\rho^{-2} - 3a^4\rho^{-4})] \sin 2\varphi. \quad (15.3)$$

The stresses  $\tilde{\sigma}_{\rho\rho}^m(\sigma_{33}^0)$ ,  $\tilde{\sigma}_{\varphi\varphi}^m(\sigma_{33}^0)$ , and  $\tilde{\sigma}_{\rho\varphi}^m(\sigma_{33}^0)$  are also given by Eqs. (15.1)–(15.3), respectively, as long as the  $\sigma_{22}^0$  in them is replaced by  $\sigma_{33}^0$  and  $\varphi$  by  $\varphi = \varphi + \pi/2$ . Substituting Eqs. (14) and (8.4) into Eq. (9), a biaxial transverse SCF of the matrix,  $K_{22}^{Bi}(\varphi)$ , is derived as

$$K_{22}^{Bi}(\varphi) = \frac{\sigma_{22}^0}{(\sigma_{22}^m)_{BM}} + \frac{A\sqrt{V_f}(\sigma_{22}^0 + \sigma_{33}^0)}{2(\sigma_{22}^m)_{BM}} \cos 2\varphi + \frac{B(\sigma_{22}^0 - \sigma_{33}^0)}{2(1 - \sqrt{V_f})(\sigma_{22}^m)_{BM}} \\ \left[ V_f^2 \cos 4\varphi + 4V_f(\cos \varphi)^2(1 - 2\cos 2\varphi) + \sqrt{V_f}(2\cos \varphi + \cos 4\varphi) \right]$$

However, the failure surface orientation of a UD composite under an equally biaxial transverse tension or compression is indeterminate. For this reason, we can assume that the failure surface orientation under an equally biaxial transverse load is the same as that under a uniaxial transverse load. In other words, we have ( $\sigma_{22}^0 = \sigma_{33}^0$ ).

$$K_{22}^{Bi,t} = K_{33}^{Bi,t} = \frac{(V_f + 0.3V_m)E_{22}^f + 0.7V_mE^m}{0.3E_{22}^f + 0.7E^m} \left( 1 + A\sqrt{V_f} \right), \text{ if } \sigma_{33}^0 > 0, \quad (16.1)$$

$$K_{22}^{Bi,c} = K_{33}^{Bi,c} = \frac{(V_f + 0.3V_m)E_{22}^f + 0.7V_mE^m}{0.3E_{22}^f + 0.7E^m} \left( 1 - A\sqrt{V_f} \frac{\sigma_{u,c}^m - \sigma_{u,t}^m}{2\sigma_{u,c}^m} \right), \text{ if } \sigma_{33}^0 < 0. \quad (16.2)$$

## 5.6 SCFs subjected to any biaxial transverse loads

When the matrix is subjected to any biaxial transverse loads, we can always separate the loads into an equally biaxial transverse tension or compression plus a uniaxial transverse tension (**Figure 3**). The SCFs of the matrix are then determined accordingly.

## 5.7 Longitudinal normal SCF

No SCF exists in such a load case, since the resulting stresses in the matrix are uniform [7, 41].

# 6. Assessment on strength prediction

## 6.1 True stresses of the matrix

Let  $\{\sigma_i^m\} = \{\sigma_{11}^m, \sigma_{22}^m, \sigma_{33}^m, \sigma_{23}^m, \sigma_{13}^m, \sigma_{12}^m\}^T$  be the homogenized stresses of the matrix in a UD composite calculated from a micromechanics model. The true stresses of the matrix,  $\{\bar{\sigma}_i^m\} = \{\bar{\sigma}_{11}^m, \bar{\sigma}_{22}^m, \bar{\sigma}_{33}^m, \bar{\sigma}_{23}^m, \bar{\sigma}_{13}^m, \bar{\sigma}_{12}^m\}^T$ , are determined as follows:

$$\{\bar{\sigma}_i^m\} = \left\{ \sigma_{11}^m, K_{33}^{Bi} \sigma_{33}^m + K_{22}^t (\sigma_{22}^m - \sigma_{33}^m), K_{33}^{Bi} \sigma_{33}^m, K_{23} \sigma_{23}^m, K_{12} \sigma_{13}^m, K_{12} \sigma_{12}^m \right\}^T, \quad (17.1)$$

if  $\sigma_{22}^m \times \sigma_{33}^m \neq 0$  and  $(\sigma_{22}^m - \sigma_{33}^m) \geq 0$ ,

$$\{\bar{\sigma}_i^m\} = \left\{ \sigma_{11}^m, K_{22}^{Bi} \sigma_{22}^m, K_{22}^{Bi} \sigma_{22}^m + K_{22}^t (\sigma_{33}^m - \sigma_{22}^m), K_{23} \sigma_{23}^m, K_{12} \sigma_{13}^m, K_{12} \sigma_{12}^m \right\}^T, \quad (17.2)$$

if  $\sigma_{22}^m \times \sigma_{33}^m \neq 0$  and  $(\sigma_{33}^m - \sigma_{22}^m) \geq 0$ ,

$$\{\bar{\sigma}_i^m\} = \left\{ \sigma_{11}^m, K_{22} \sigma_{22}^m, 0, K_{23} \sigma_{23}^m, K_{12} \sigma_{13}^m, K_{12} \sigma_{12}^m \right\}^T, \text{ if } \sigma_{33}^m = 0, \quad (18.1)$$

$$\{\bar{\sigma}_i^m\} = \left\{ \sigma_{11}^m, 0, K_{33} \sigma_{33}^m, K_{23} \sigma_{23}^m, K_{12} \sigma_{13}^m, K_{12} \sigma_{12}^m \right\}^T, \text{ if } \sigma_{22}^m = 0, \quad (18.2)$$

$$K_{22}^{Bi} = \begin{cases} K_{22}^{t, Bi}, & \text{if } \sigma_{22}^m > 0 \\ K_{22}^{c, Bi}, & \text{if } \sigma_{22}^m < 0 \end{cases}, \quad (19.1)$$

$$K_{33}^{Bi} = \begin{cases} K_{22}^{t, Bi}, & \text{if } \sigma_{33}^m > 0 \\ K_{22}^{c, Bi}, & \text{if } \sigma_{33}^m < 0 \end{cases}, \quad (19.2)$$

$$K_{22} = \begin{cases} K_{22}^t, & \text{if } \sigma_{22}^m > 0 \\ K_{22}^c, & \text{if } \sigma_{22}^m < 0 \end{cases}, \quad (19.3)$$

$$K_{33} = \begin{cases} K_{22}^t, & \text{if } \sigma_{33}^m > 0 \\ K_{22}^c, & \text{if } \sigma_{33}^m < 0 \end{cases}. \quad (19.4)$$

## 6.2 Uniaxial strength formulae

Bridging tensor elements of a micromechanics model for each of the nine UD composites can be calculated through Eq. (6), using the corresponding elastic moduli given in **Table B.3**.

Under a uniaxial load, only the internal stress component of a constituent (fiber or matrix) along the loading direction is dominant. The other stress components, if any, are negligibly small. This can be realized from the explicit Eqs. (8.1)–(8.6). Accordingly, a longitudinal failure of the composite is controlled mostly by a fiber failure, whereas all of the other failures are resulted from matrix failures. We only need to determine the following relationships:

$$\sigma_{11}^f = \lambda_1 \sigma_{11}^0, \sigma_{22}^m = \lambda_2 \sigma_{22}^0, \sigma_{23}^m = \lambda_3 \sigma_{23}^0, \sigma_{12}^m = \lambda_4 \sigma_{12}^0. \quad (20)$$

where  $\lambda_i$ s are dependent on the bridging tensor and  $\sigma_{11}^0$ ,  $\sigma_{22}^0$ ,  $\sigma_{23}^0$ , and  $\sigma_{12}^0$  are external loads applied individually to the composite once at a time. For each of the 9 composites, the  $\lambda_i$ s calculated by the 12 models are summarized in **Table B.4**.

In terms of the data in **Table B.4**, the longitudinal tensile and compressive, transverse tensile and compressive, transverse shear, and longitudinal shear strengths of a UD composite are estimated through.

$$\begin{aligned} \sigma_{11}^{u,t} &= \sigma_{u,t}^f / \lambda_1, \sigma_{11}^{u,c} = \sigma_{u,c}^f / \lambda_1, \sigma_{22}^{u,t} = \sigma_{u,t}^m / (K_{22}^t \lambda_2), \sigma_{22}^{u,c} = \sigma_{u,c}^m / (K_{22}^c \lambda_2), \\ \sigma_{23}^u &= \sigma_{u,s}^m / (K_{23} \lambda_3), \text{ and } \sigma_{12}^u = \sigma_{u,s}^m / (K_{12} \lambda_4) \end{aligned} \quad (21)$$

where  $K_{22}^t$ ,  $K_{22}^c$ ,  $K_{12}$ , and  $K_{23}$  are the transverse tensile, transverse compressive, longitudinal shear, and transverse shear SCFs of the matrix in the composite.

	E-glass LY556	E-glass MY750	AS4 3501-6	T300 BSL914C	IM7 8511-7	T300 PR319	AS epoxy	S2-glass epoxy	G400-800 5260
$K_{12}$	1.52	1.491	1.424	1.43	1.475	1.51	1.449	1.5	1.483
$K_{23}$	3.02	2.936	1.337	2.421	2.034	2.167	1.999	2.982	2.469
$K_{22}^t$	3.339	3.253	2.098	2.143	2.327	3.123	2.339	3.317	2.464
$K_{22}^c$	2.249	2.181	1.469	1.57	1.761	2.035	1.743	2.172	1.732
$K_{22}^{Bi,t}$	2.747	2.67	1.743	1.759	1.905	2.55	1.916	2.719	2.08
$K_{22}^{Bi,c}$	2.182	2.132	1.562	1.601	1.712	2.05	1.709	2.148	1.74

**Table 2.**  
SCFs of the matrices in the nine composites.

### 6.3 Prediction assessment

Using the constituent data of **Table B.1**, all of the SCFs of the matrices in the nine composites are calculated as per Eqs. (12), (13), and (16). They are listed in **Table 2**. All of the SCFs only depend on the constituent properties and fiber volume fraction of a composite, since a perfect interface bonding has been implicitly assumed. **Table 2** shows that the transverse tensile SCF of the matrix is generally the biggest in a composite, whereas the transverse shear SCF is the second biggest or even bigger than all of the remaining SCFs in some composite. Further, the transverse tensile SCF can be greater than 3, implying that the classical SCF of a plate with a hole is not the upper limit for that of the matrix when the hole is filled with a fiber.

The predicted results are compared with the experimental measurements shown in **Table B.2**, and the averaged relative correlation errors for all of the 12 models are summarized in **Table 3**. It shows that Bridging Model is still overall the most accurate, although the accuracy difference between Bridging Model and the other

Model	$N$	Averaged error*	Error ratio	Rank	Model	$N$	Averaged error*	Error ratio	Rank
Bridging model	53	21.1%	1.0	1	Mori-Tanaka method	53	30.2%	1.43	8
Double inclusion (Digimat)	53	21.9%	1.04	2	Modified rule of mixture	53	30.7%	1.45	10
FE-square	53	23.1%	1.09	3	FE-square diagonal	53	31.9%	1.51	11
Chamis model	53	25.4%	1.20	4	FE-hexagonal	53	32%	1.52	12
FE-random	53	28.5%	1.30	5	Self-consistent method	53	32.7%	1.54	13
Hill-Hashin-C-L model	18	30.1%	1.43	6	Rule of mixture method	53	44.5%	2.11	14
Halpin-Tsai formulae	53	30.1%	1.43	6	Eshelby's method	53	45.1%	2.14	15
Generalized self-consistent	53	30.2%	1.43	8					

$$* = \frac{1}{N} \sum_{i=1}^N \text{abs}(\text{error})_i.$$

**Table 3.**  
Overall averaged errors in prediction of the uniaxial strengths of the nine UD composites by different models.

top three models is insignificant. Compared **Table 3** with **Table 1**, the ranking order of the top four theories for both the stiffness and strength predictions is essentially the same, with only a minor difference in the ranking order from stiffness and strength predictions by the FE-square and double inclusion method.

The largest correlation error in the strength prediction is still assumed by Eshelby's method, which is 45.1%. Another model gaining a correlation error of more than 40% is rule of mixture method. All of the theories under consideration for the strength predictions can be classified into three classes, according to their accuracies attained. The first class exhibits the highest accuracy. It consists of four methods, which are Bridging Model, double inclusion method, the FE-square, and Chamis model, with a correlation error in between 21.1% and 25.4%. The second class is moderate in accuracy performance. Most of the models, i.e., the FE-random, Hill-Hashin-Christensen-Lo model, Halpin-Tsai formulae, generalized self-consistent method, Mori-Tanaka method, modified rule of mixture method, the FE-square diagonal, the FE-hexagonal and self-consistent method, are within this class. Their correlation errors vary from 27.4% to 32.7%. The third class possesses the lowest prediction accuracy, consisting of two models, i.e., rule of mixture method and Eshelby's method. Looking back at **Table 1**, the classification of the three classes of the micromechanics models for the stiffness predictions is also valid.

If no SCFs of the matrix are taken into account, i.e., if  $K_{22}^t = K_{22}^c = K_{12} = K_{23} \equiv 1$  are assumed in Eq. (21), the overall correlation error by a model from the first or the second class is much greater. Consider, e.g., Bridging Model. Without the SCFs, the correlation error between the predicted and measured transverse tensile, transverse compressive, transverse shear, and longitudinal shear strengths of the 9 composites is 115.3%, 5.22 times greater than that when the SCFs are taken into account. It is noted that the longitudinal strength predictions have been excluded in this latter comparison. Hence, the most critical factor to influence the overall strength prediction is the SCFs of the matrix in the composite.

## 7. Additional comments

### 7.1 Consistency

Eqs. (1)–(6) are valid for both 2D and 3D stress states. Any micromechanics model can result in two sets of internal stress formulae, i.e., 2D and 3D formulae, respectively. Let the composite be subjected to a planar stress state  $\{\sigma_{11}^0, \sigma_{22}^0, \sigma_{12}^0\}$ . The resulting internal stresses in the fiber and matrix by the 2D formulae are represented as  $\{\sigma_{11}^{f,2D}, \sigma_{22}^{f,2D}, \sigma_{33}^{f,2D}, \sigma_{23}^{f,2D}, \sigma_{13}^{f,2D}, \sigma_{12}^{f,2D}\}$  and  $\{\sigma_{11}^{m,2D}, \sigma_{22}^{m,2D}, \sigma_{33}^{m,2D}, \sigma_{23}^{m,2D}, \sigma_{13}^{m,2D}, \sigma_{12}^{m,2D}\}$ , where  $\sigma_{33}^{f,2D} = \sigma_{23}^{f,2D} = \sigma_{13}^{f,2D} = \sigma_{33}^{m,2D} = \sigma_{23}^{m,2D} = \sigma_{13}^{m,2D} = 0$ . On the other hand, using the 3D stress formulae and applying a load combination  $\{\sigma_{11}^0, \sigma_{22}^0, 0, 0, 0, \sigma_{12}^0\}$ , the internal stresses thus obtained are denoted as  $\{\sigma_{11}^{f,3D}, \sigma_{22}^{f,3D}, \sigma_{33}^{f,3D}, \sigma_{23}^{f,3D}, \sigma_{13}^{f,3D}, \sigma_{12}^{f,3D}\}$  and  $\{\sigma_{11}^{m,3D}, \sigma_{22}^{m,3D}, \sigma_{33}^{m,3D}, \sigma_{23}^{m,3D}, \sigma_{13}^{m,3D}, \sigma_{12}^{m,3D}\}$ . If  $\sigma_{ij}^{f,2D} = \sigma_{ij}^{f,3D}$  and  $\sigma_{ij}^{m,2D} = \sigma_{ij}^{m,3D}$  for all  $i$  and  $j$ , the corresponding micromechanics model is said to be consistent in the internal stress calculation.

A necessary and sufficient condition for a micromechanics model to be consistent is that its bridging tensor is always in an upper triangular form. If, e.g.,  $A_{32} \neq 0$ , we will get from Eqs. (3) and (4) that  $\sigma_{33}^f = B_{32}\sigma_{22}^0 \neq 0$  and  $\sigma_{33}^m = A_{32}\sigma_{22}^f + A_{33}\sigma_{33}^f \neq 0$ , where  $[B_{ij}] = (V_f[I] + V_m[A_{ij}])^{-1}$ . The bridging tensor of Bridging Model, by

definition, is always upper triangular, even when a constituent, e.g., matrix undergoes a plastic deformation [16]. On the other hand, the bridging tensors of all of the other models for the nine composites are not upper triangular. Hence, all of the other models are not consistent. The non-consistency implies that the homogenized internal stresses should be calculated using the full 3D stress formulae, even though the composite is subjected to a uniaxial load. To apply an analytical model, other than Bridging Model, the 3D compliance tensors of the fiber, matrix, and the composite should be used in Eq. (6) to obtain the 3D bridging tensor. If a numerical method is applied to predict a composite property, a 3D rather than 2D RVE geometry should be discretized.

## 7.2 Accuracy estimation

It is known that the elasticity of UD composites is essentially matured. This means that the accuracy in both experimental measurement and micromechanics prediction for the elastic properties of a UD composite is likely not improvable significantly, unless a revolutionary change in the processing technology for a composite occurs. Considering the measurement deviations for the fiber, matrix, and composite properties as well as for the fiber volume fraction and in light of **Table 1**, it can draw a conclusion that an overall correlation error of 10% would be the one attainable in the composite stiffness prediction if only the original constituent information is available. As more than double of the constituent data together with more other information are required in a strength prediction, a reasonable correlation error in this latter case that can be expected should be more than 10% and mostly up to 20%.

The individual correlation error for each of the uniaxial strengths of the nine UD composites by Bridging Model is calculated and is shown in **Table 4**. Evidently, the predictions by the current theory for the longitudinal tensile, longitudinal shear, and transverse shear strengths of the composites are good enough, whereas those for the other three strength properties are either bad or not very satisfactory. Improvement in the prediction accuracy for the latter three uniaxial strengths is expected.

## 7.3 Improvement in strength prediction

From **Table 4**, the largest correlation error comes from the prediction of a transverse tensile strength. This is attributed to a crack occurred in between the fiber and matrix interface. There must be some composites in which the fiber and matrix interfaces were already debonded before an ultimate failure under a transverse tensile load. Many researches in the literature have confirmed that an interface debonding has the greatest influence on the transverse tensile strength of a composite [42–44]. Therefore, a true stress component of the matrix corresponding to a transverse tension must take an interface debonding into account [11].

The second largest error is in the prediction of a longitudinal compressive strength. Only a strength failure has been considered in this work for a composite

Longitudinal tensile strength	Longitudinal compressive strength	Longitudinal shear strength	Transverse tensile strength	Transverse compressive strength	Transverse shear strength	Overall
11%	25.1%	13.1%	39.2%	23.2%	14.3%	21.1%

**Table 4.**

*Averaged correlation errors of Bridging Model for the individual uniaxial strengths of the nine UD composites.*

subjected to a longitudinal compression. Existing evidences show that a longitudinal compressive failure is frequently caused by a kink-band or microbuckling [45–47], due to an initial fiber misalignment. A micromechanics approach for a kink-band failure only using the original fiber and matrix properties together with the initial fiber misalignment angle has been achieved very recently [48]. However, a fiber misalignment angle is in most cases an in situ parameter and is difficult to be accurately measured. A more suitable way is to retrieve it from a measured longitudinal compressive strength parameter of the composite. On the other hand, this parameter can also be used to adjust the fiber compressive strength to improve the correlation accuracy.

The third correlation error, which is greater than 20%, occurs in the prediction for the transverse compressive strengths of the composites. Most probably, this error is attributed mainly to an inaccurate measurement/determination of a matrix compressive strength. It is known that among the three uniaxial strength parameters of a matrix especially a ductile polymer or metal matrix material, the compressive strength is the most difficult to be measured. Sometimes, one even cannot obtain a fracture load when a cylinder sample is compressively tested. Further study is needed to determine a matrix compressive strength.

An interesting phenomenon behind **Table 4** is that either longitudinal or transverse shear strength can be sufficiently well predicted based on a perfect interface bonding assumption. Undoubtedly, an interface debonding may occur when the composite is subjected to a shear load. But the interface debonding has insignificant effect on the shear as well as on any other kind of load carrying ability of a composite except for the transverse tension, as seen in the subsequent section.

## 8. Failure prediction with a debonded interface

### 8.1 Transverse tensile SCF of the matrix after interface crack

All of the SCFs presented in the preceding section are based on an assumption that the fiber and matrix interface has a perfect bonding up to a composite failure. In other words, the point-wise displacements and the point-wise stresses of the fiber and matrix on their common boundary are continuous. In most cases, an interface debonding or crack can occur before an ultimate failure of the composite. However, **Table 4** suggests that only the transverse tensile load sustaining ability of the composite is influenced heavily by the interface crack or debonding. The transverse tensile SCF of the matrix after the interface crack (**Figure 4**) must be taken into account in a failure prediction, in general. This SCF has been derived in Ref. [11], which is summarized below.

$$\hat{K}_{22}^t = \hat{K}_{22}^t(\psi) = \text{Re} \left\{ e^{-2i\psi} M(b e^{i\psi}) (a^2/b - b) - e^{-i\psi} \left( N_2 - N_1 \left( \frac{a^2}{b} e^{-i\psi} \right) \right) + e^{-i\psi} (2 + e^{-2i\psi}) [N(b e^{i\psi}) - N_3] \right\} \frac{(V_f + 0.3V_m)E_{22}^f + 0.7V_m E^m}{2(b - a)(0.3E_{22}^f + 0.7E^m)}, \quad (22.1)$$

$$N(z) = Fz + \frac{a^2 k}{z} - (z - a e^{i\psi})^{0.5+i\lambda} (z - a e^{-i\psi})^{0.5-i\lambda} \left[ (F - 0.5) - \frac{D}{a^2 z} \right], \quad (22.2)$$

$$N_1(z) = Fz + \frac{a^2 k}{z} + \frac{1}{\xi} (z - a e^{i\psi})^{0.5+i\lambda} (z - a e^{-i\psi})^{0.5-i\lambda} \left[ (F - 0.5) - \frac{D}{a^2 z} \right], \quad (22.3)$$

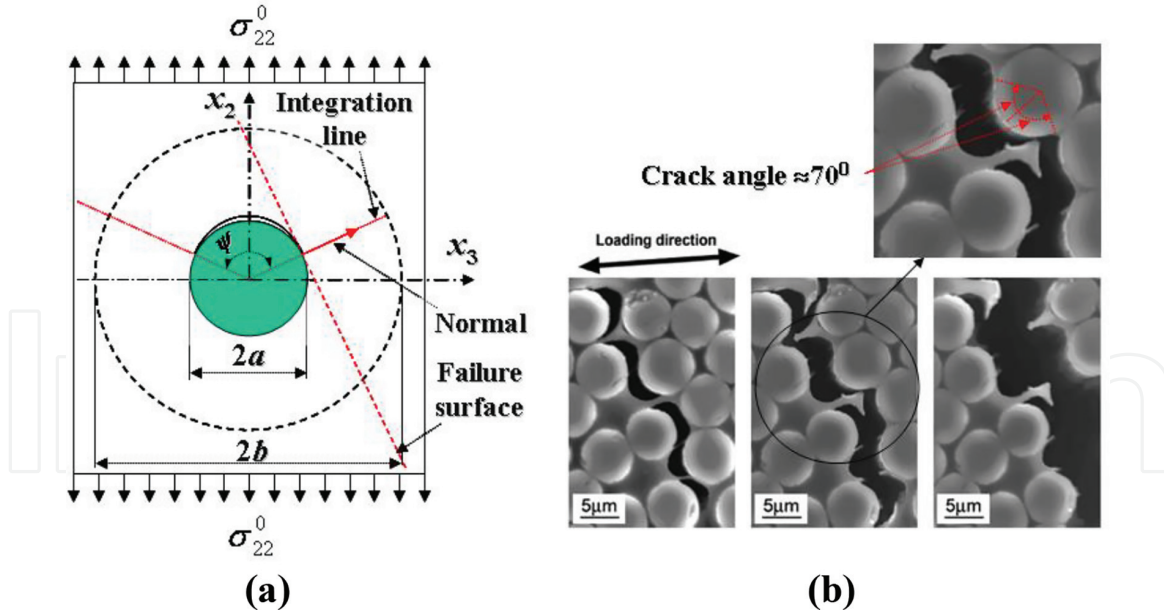


**Figure 4.** (a) Schematic failure of a transverse tensile-loaded composite with an interface crack, (b) failure locus of a composite after interface cracks [42].

$$N_2 = aFe^{-i\psi} + ake^{i\psi}, N_3 = Fae^{i\psi} + e^{-i\psi}ak, \quad (22.4)$$

$$M(z) = F - \frac{a^2k}{z^2} - \left[ (F - 0.5)z + H + \frac{C}{z} + \frac{D}{z^2} \right] \chi(z), \quad (22.5)$$

$$F = \frac{1 - (\cos \psi + 2\lambda \sin \psi) \exp [2\lambda(\pi - \psi)] + (1 - k)(1 + 4\lambda^2) \sin^2 \psi}{\frac{4}{k} - 2 - 2(\cos \psi + 2\lambda \sin \psi) \exp [2\lambda(\pi - \psi)]}, \quad (22.6)$$

$$H = a(\cos \psi + 2\lambda \sin \psi)(0.5 - F), \quad (22.7)$$

$$C = (k - 1)(\cos \psi - 2\lambda \sin \psi)a^2 \exp [2\lambda(\psi - \pi)], \quad (22.8)$$

$$D = (1 - k)a^3 \exp [2\lambda(\psi - \pi)], \quad (22.9)$$

$$\chi(z) = (z - ae^{i\psi})^{-0.5+i\lambda} (z - ae^{-i\psi})^{-0.5-i\lambda}, \quad (22.10)$$

$$k = \frac{G^m(1 + \kappa_2)}{(1 + \xi)(G^m + \kappa_1 G_{23}^f)}, \lambda = -(\ln \xi)/(2\pi), \xi = (G_{23}^f + \kappa_2 G^m)/(G^m + \kappa_1 G_{23}^f),$$

$$\kappa_1 = 3 - 4\nu^m, \kappa_2 = \frac{3 - \nu_{23}^f - 4\nu_{12}^f \nu_{21}^f}{1 + \nu_{23}^f}, \quad (22.11)$$

$$b = a / \sqrt{V_f}. \quad (22.12)$$

In the above,  $\psi$  is the half of the crack angle, which is determined from

$$\operatorname{Re} \left\{ \left( G_0 - \frac{1}{k} - \frac{2(1-k)}{k \exp(i\varphi)} \exp [2\lambda(\psi - \pi)] \right) R(e^{i\varphi}) \right\}_{\varphi=\psi-\gamma} = 0, \quad (23.1)$$

$$R(\exp(i\varphi)) = [\exp(i\varphi) - e^{i\psi}]^{0.5+i\lambda} [\exp(i\varphi) - e^{-i\psi}]^{0.5-i\lambda} \exp(-i\varphi), \quad (23.2)$$

$$G_0 = \frac{1 - (\cos \psi + 2\lambda \sin \psi) \exp [2\lambda(\pi - \psi)] + (1 - k)(1 + 4\lambda^2) \sin^2 \psi}{2 - k - k(\cos \psi + 2\lambda \sin \psi) \exp [2\lambda(\pi - \psi)]}, \quad (23.3)$$

$$\gamma = \begin{cases} \frac{2\lambda(J_1^2 + J_2^2)}{J_1^2 + J_2^2 - 2J_2J_3}, & \text{if } \xi < 1 \\ -\frac{2\lambda(J_1^2 + J_2^2)}{J_1^2 + J_2^2 - 2J_2J_3}, & \text{if } \xi > 1 \end{cases}, \quad (23.4)$$

$$J_1 = kG_0 - 1 - 2(1 - k)\xi \exp (2\lambda\psi) \cos (\psi), \quad (23.5)$$

$$J_2 = 2(1 - k)\xi \exp (2\lambda\psi) \sin (\psi), \quad (23.6)$$

$$J_3 = 2(1 - k)\xi \exp (2\lambda\psi) [J_1 \cos (\psi) - J_2 \sin (\psi)] / J_2. \quad (23.7)$$

If  $\xi = 1$ , no solution for  $\psi$  is obtainable from Eq. (23). The corresponding interface crack is called a singular crack. But one can always adjust the fiber or the matrix properties involved so that  $\xi \neq 1$ , since experimental deviations exist in measurement of them.

## 8.2 Interface crack detection

Let a UD composite be subjected to a transverse tension,  $\sigma_{22}^0$ , up to an ultimate failure. The measured transverse tensile strength of the composite is  $Y$ . Suppose that the fiber/matrix interface of the composite is initially bonded perfectly. When the load is increased to a critical level, e.g.,  $\hat{\sigma}_{22}^0$ , a stable crack with a central angle of  $2\psi$  occurs on the interface. Many reports have pointed out that an unstable propagation from an initial interface crack to the last stable angle is short [42, 49, 50], with no significant change in the applied load. Thus, we can safely assume that at a transverse load level smaller than  $\hat{\sigma}_{22}^0$  the interface is in perfect bonding.

From Eq. (8.4), the transverse stress in the matrix when the crack occurs reads

$$\hat{\sigma}_{22}^m = \frac{0.3E_{22}^f + 0.7E^m}{(V_f + 0.3V_m)E_{22}^f + 0.7V_mE^m} \hat{\sigma}_{22}^0. \quad (24.1)$$

Further, the longitudinal stress of the matrix at the critical load level is obtained from Eq. (8.2) as

$$\hat{\sigma}_{11}^m = \frac{V_f a_{12}}{(V_f + V_m a_{11})(V_f + V_m a_{22})} \hat{\sigma}_{22}^0. \quad (24.2)$$

No other stress in the matrix exists. Supposing that the transverse matrix stress corresponding to the composite failure is denoted by  $\bar{\bar{\sigma}}_{22}^m$ , one has.

$$\hat{K}_{22}^t (\bar{\bar{\sigma}}_{22}^m - \hat{\sigma}_{22}^m) + K_{22}^t \hat{\sigma}_{22}^m = \sigma_{u,t}^m, \quad (25.1)$$

where

$$\bar{\bar{\sigma}}_{22}^m - \hat{\sigma}_{22}^m = \frac{0.3E_{22}^f + 0.7E^m}{(V_f + 0.3V_m)E_{22}^f + 0.7V_mE^m} (Y - \hat{\sigma}_{22}^0). \quad (25.2)$$

From Eqs. (24.1), (25.1), and (25.2), the critical transverse tensile load is found to be

$$\hat{\sigma}_{22}^0 = \frac{\hat{K}_{22}^t Y^t}{\hat{K}_{22}^t} - K_{22}^t - \frac{(V_f + 0.3V_m)E_{22}^f + 0.7V_mE^m}{(0.3E_{22}^f + 0.7E^m)(\hat{K}_{22}^t - K_{22}^t)} \sigma_{u,t}^m. \quad (26)$$

If it is equal to or greater than the transverse tensile strength,  $Y$ , the fiber and matrix system is said to have a perfect interface bonding up to failure. Otherwise, the system will undergo an earlier interface crack and a further interface modification is preferred.

Under any arbitrary load condition, an interface crack occurs in the composite if and only if

$$(\bar{\sigma}_m^1)_l > 0 \quad (27.1)$$

and

$$(\bar{\sigma}_e^m)_l \geq \hat{\sigma}_e^m, \quad (27.2)$$

where

$$\hat{\sigma}_e^m = \sqrt{(\hat{\sigma}_{11}^m)^2 + (K_{22}^t \hat{\sigma}_{22}^m)^2 - K_{22}^t \hat{\sigma}_{11}^m \hat{\sigma}_{22}^m} \quad (28)$$

is the critical Mises stress.  $(\bar{\sigma}_e^m)_l$  and  $(\bar{\sigma}_m^1)_l$  are the Mises and the first principal stresses of the matrix obtained from the current load-step true stresses. For instance, when a planar load is applied to the composite, the current Mises true stress is given by

$$(\bar{\sigma}_e^m)_l = \sqrt{(\bar{\sigma}_{11}^m)_l^2 + (\bar{\sigma}_{22}^m)_l^2 - (\bar{\sigma}_{11}^m)_l (\bar{\sigma}_{22}^m)_l + 3(\bar{\sigma}_{12}^m)_l^2}, \quad (29)$$

$$(\bar{\sigma}_{11}^m)_l = (\bar{\sigma}_{11}^m)_{l-1} + d\sigma_{11}^m, \quad (30.1)$$

$$(\bar{\sigma}_{22}^m)_l = (\bar{\sigma}_{22}^m)_{l-1} + K_{22}^{eq} d\sigma_{22}^m, \quad (30.2)$$

$$(\bar{\sigma}_{12}^m)_l = (\bar{\sigma}_{12}^m)_{l-1} + K_{12} d\sigma_{12}^m, \quad (30.3)$$

$$K_{22}^{eq} = \begin{cases} K_{22}^t, & \text{if } d\sigma_{22}^m > 0 \text{ and } (\bar{\sigma}_e^m)_{l-1} < \hat{\sigma}_e^m \\ \hat{K}_{22}^t, & \text{if } d\sigma_{22}^m > 0 \text{ and } (\bar{\sigma}_e^m)_{l-1} \geq \hat{\sigma}_e^m \\ K_{22}^c, & \text{if } d\sigma_{22}^m < 0 \end{cases}. \quad (31)$$

The homogeneous stress increments,  $\{d\sigma_{11}^m, d\sigma_{22}^m, d\sigma_{12}^m\}$ , are calculated from Eqs. (8.2) and (8.4) in which  $\{\sigma_{11}^0, \sigma_{22}^0, \sigma_{12}^0\}$  are replaced by  $\{d\sigma_{11}^0, d\sigma_{22}^0, d\sigma_{12}^0\}$ .

Using the data of **Tables B.1** and **B.2**, the transverse tensile SCFs of the nine UD composites after the interface crack together with the crack (half) angles are

	E-glass LY556	E-glass MY750	AS4 3501-6	T300 BSL914C	IM7 8551-7	T300 PR319	AS epoxy	S2-glass epoxy	G40-800 5260
$\hat{K}_{22}^t$	7.69	7.22	4.95	5.04	5.41	6.97	5.43	7.34	5.68
$\psi$	71.8°	71.9°	73.9°	73.9°	73.4°	72°	73.3°	71.8°	72.8°
$\hat{\sigma}_{22}^0$ (MPa)	20.3	28.2	44.4	4.7	72.5	33.5	19	74.3	93.2
$\hat{\sigma}_e^m$ (MPa)	28.6	39.8	53.9	5.76	90.6	46.3	24	105.1	119.4

**Table 5.**

Transverse tensile SCFs and other relevant parameter of the nine composites after interface debonding.

calculated from Eqs. (22) and (23). The critical transverse and Mises stresses are also obtained from Eqs. (26) and (28), respectively. They are summarized in **Table 5**. It is seen that the half crack angles of the carbon and glass fiber matrix interfaces under a transverse tension are close to 70°, consistent with the measured result shown in **Figure 4b**. Comparing the resulting  $\hat{\sigma}_{22}^0$  with the corresponding measured transverse tensile strengths, one can see that four composites, i.e., AS4/3501-6, IM7/8551-7, S2-Glass/Epoxy, and G40-800/5260 systems, have or nearly have a perfect interface bonding up to failure. The remaining five composites will undergo an interface debonding early before failure. There are two composite systems, S2-Glass/Epoxy and G40-800/5260, having a more than enough interface bonding strength, implying that more than enough efforts might have been paid.

### 8.3 Off-axial strength prediction

A composite strength is assumed if either a fiber or a matrix failure is attained. A matrix failure is detected through, e.g., Tsai-Wu's criterion (as isotropic materials are a subset of anisotropic composites), whereas a fiber failure is assessed by the generalized maximum normal stress failure criteria [16], through the following expressions:

$$F_1 \left[ (\bar{\sigma}_{11}^m)_l^2 + (\bar{\sigma}_{22}^m)_l^2 - (\bar{\sigma}_{11}^m)_l (\bar{\sigma}_{22}^m)_l \right] + F_2 (\bar{\sigma}_{12}^m)_l^2 + F_3 \left[ (\bar{\sigma}_{11}^m)_l + (\bar{\sigma}_{22}^m)_l \right] \geq 1, \quad (32.1)$$

$$F_1 = 1/(\sigma_{u,t}^m \sigma_{u,c}^m), F_2 = 1/(\sigma_{u,s}^m)^2, F_3 = 1/\sigma_{u,t}^m - 1/\sigma_{u,c}^m. \quad (32.2)$$

$$(\sigma_{eq,t}^f)_l \geq \sigma_{u,t}^f \text{ or } (\sigma_{eq,c}^f)_l \geq -\sigma_{u,c}^f \quad (33.1)$$

$$(\sigma_{eq,t}^f)_l = \begin{cases} (\sigma_f^1)_l, & \text{if } (\sigma_f^3)_l < 0, \\ \left[ (\sigma_f^1)_l^3 + (\sigma_f^2)_l^3 \right]^{1/3}, & \text{if } (\sigma_f^3)_l = 0 \end{cases}, \quad (33.2)$$

$$(\sigma_{eq,c}^f)_l = \begin{cases} (\sigma_f^3)_l, & \text{if } (\sigma_f^1)_l > 0, \\ (\sigma_f^3)_l - (\sigma_f^1)_l, & \text{if } (\sigma_f^1)_l \leq 0 \end{cases}. \quad (33.3)$$

$(\sigma_f^1)_l$ ,  $(\sigma_f^2)_l$ , and  $(\sigma_f^3)_l$  ( $\sigma_f^1 \geq \sigma_f^2 \geq \sigma_f^3$ ) are the three principal stresses of the fiber calculated from

$$(\sigma_{11}^f)_l = (\sigma_{11}^f)_{l-1} + d\sigma_{11}^f, \quad (34.1)$$

$$(\sigma_{22}^f)_l = (\sigma_{22}^f)_{l-1} + d\sigma_{22}^f, \quad (34.2)$$

$$(\sigma_{12}^f)_l = (\sigma_{12}^f)_{l-1} + d\sigma_{12}^f. \quad (34.3)$$

$\sigma_{u,t}^f$  and  $\sigma_{u,c}^f$  are longitudinal tensile and compressive strengths of the fiber, respectively.

Two UD composites, Kevlar-49/epoxy and E-glass/8804 epoxy systems, were subjected to off-axial tensile load up to failure. Constituent properties and transverse tensile strengths of the two composites as well as fiber volume fractions were provided in Ref. [51, 52] and cited in **Table 6**. From them, the SCFs of the matrices and the critical Mises stresses can be calculated and are also shown in the table. The predicted off-axial strengths of the Kevlar-49/epoxy and E-glass/8804 composites

	$E_{11}^f$ (GPa)	$E_{22}^f$ (GPa)	$G_{12}^f$ (GPa)	$\nu_{12}^f$	$\nu_{23}^f$	$\sigma_{u,t}^f$ (GPa)	$E^m$ (GPa)	$\nu^m$	$\sigma_{u,t}^m$ (MPa)	$\sigma_{u,c}^m$ (MPa)	$\sigma_{u,s}^m$ (MPa)	$V_f$	$K_{22}^t$	$K_{22}^c$	$\hat{K}_{22}^t$	$K_{12}$	$\hat{\sigma}_e^m$ (MPa)
Kevlar-49/ epoxy	124.1	4.1	2.9	0.35	0.35	2.06	3.45	0.35	69	120	50	0.55	1.08	1.07	2.74	1.17	1.1
E-glass/ 8804	71	71	28.2	0.26	0.26	1.5	3.1	0.29	70	86	39	0.51	2.97	2.02	5.6	1.38	59.6

**Table 6.**  
Constituent properties and resulting matrix parameters of two UD composites [51, 52].

are plotted in **Figures 5** and **6**, respectively. The SCFs in the Kevlar fiber system with a perfect interface bonding are close to 1, because the transverse modulus of the Kevlar fiber is comparable to that of the matrix. Nevertheless, the transverse tensile SCF of the matrix in the Kevlar fiber system after the interface crack is still significantly higher than that with the perfect interface bonding. Both of the critical transverse loads of the composites,  $\hat{\sigma}_{22}^0 = 1.2$  MPa for the Kevlar and  $\hat{\sigma}_{22}^0 = 42.4$  MPa for the glass composites, are smaller than the corresponding transverse tensile strengths, 27.7 and 45.3 MPa, respectively, and the two composites will undergo an interface crack. However, the Kevlar fiber system will crack much earlier than the E-glass fiber system does when subjected to a transverse tensile load.

Given an off-axial tensile load increment,  $d\sigma_\theta$ , where  $\theta$  is the off-axial angle, the stress increments  $\{d\sigma_{11}^0, d\sigma_{22}^0, d\sigma_{12}^0\}$  are obtained through a coordinate transformation, and the interface cracking load,  $\hat{\sigma}_\theta^0$ , can be determined through Eq. (27). Consider the Kevlar fiber composite, for instance, and take  $\theta = 30^\circ$ . The homogenized stresses of the matrix are obtained from Eqs. (8.2), (8.4), and (8.6) as  $\sigma_{11}^m = 0.115\sigma_\theta$ ,  $\sigma_{22}^m = 0.234\sigma_\theta$ , and  $\sigma_{12}^m = -0.32\sigma_\theta$ , whereas the true stresses before the interface crack are  $\bar{\sigma}_{11}^m = 0.115\sigma_\theta$ ,  $\bar{\sigma}_{22}^m = 0.253\sigma_\theta$ , and  $\bar{\sigma}_{12}^m = -0.374\sigma_\theta$ . Hence, the interface cracking load  $\hat{\sigma}_{30^\circ}^0 = 1.11/0.684 = 1.623$  MPa.

After the interface crack, only the transverse tensile stress increment of the matrix will be amplified with a different SCF. The true stresses of the matrix in the Kevlar fiber composite with  $\theta = 30^\circ$  and after the interface crack are given by  $\bar{\sigma}_{11}^m = 0.115\sigma_\theta$ ,  $\bar{\sigma}_{22}^m = 0.41 + 0.641(\sigma_\theta - 1.623)$ , and  $\bar{\sigma}_{12}^m = -0.374\sigma_\theta$ . As the matrix failure occurs first, the predicted ultimate off-axial tensile strength from Eq. (32) is  $\sigma_{30^\circ}^{u,t} = 80.5$  MPa, very close to the measured one, 83.4 MPa [53].

The measured data for the Kevlar and the glass composites taken from Pindera et al. [53] and Mayes et al. [52] are also shown on **Figures 5** and **6**, respectively. In order to display the predicted results at most off-axial angles more clearly, the predictions at angles smaller than  $10^\circ$  are not included in the figures. Three kinds of predictions have been made. One is with a perfect interface bonding assumption, another without any SCF of the matrix considered, and the third is incorporated with an interface crack. As expected, the predictions without any SCF are far away from the experiments at most off-axial angles, whereas those with the interface

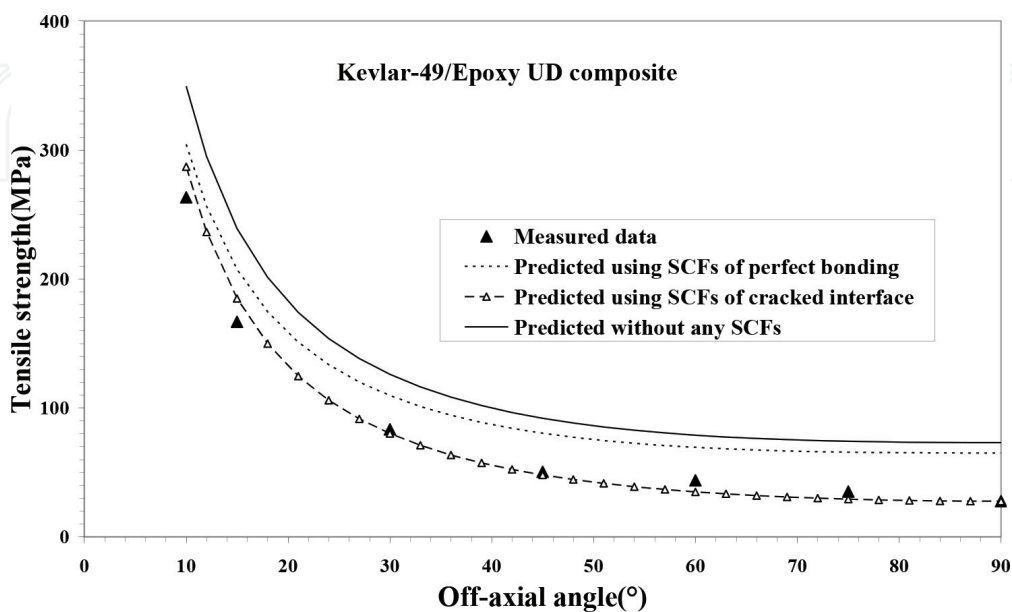


**Figure 5.** Comparison of different schemes' predictions with experiments [53] for off-axial tensile strengths of a Kevlar-49/epoxy UD composite.

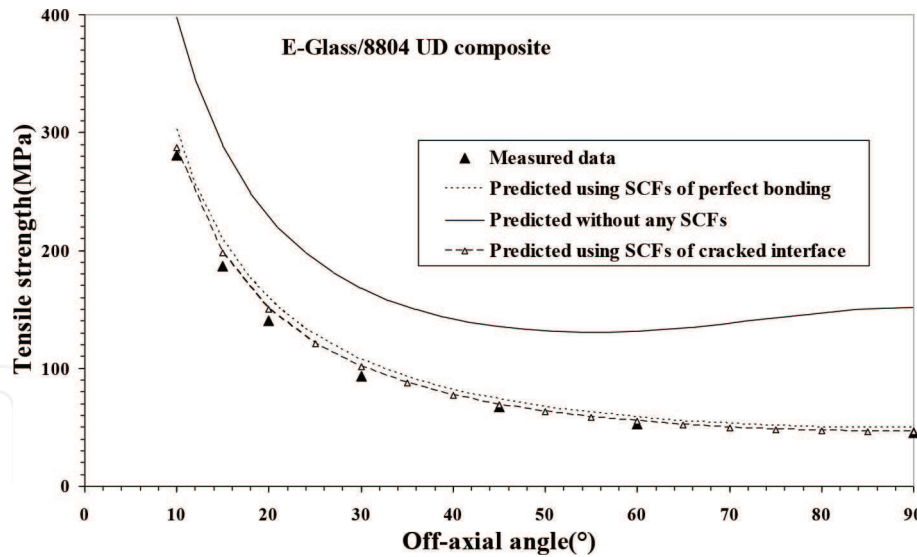


**Figure 6.**

Comparison of different schemes' predictions with experiments [53] for off-axis tensile strengths of an E-glass/8804 UD composite.

crack incorporated agree the best with the measured data. The perfect bonding assumption for both of the composites results in the predictions lied in between the other two kinds of predictions. Whereas the perfect bonding assumption up to a composite failure for the E-glass fiber system is good enough (**Figure 6**), the same assumption for the Kevlar fiber system generates significant prediction errors in general (**Figure 5**). This is because the E-glass fiber system under consideration has a critical transverse load (42.4 MPa) quite close to the transverse tensile strength, 45.3 MPa. On the other hand, the Kevlar fiber system can only sustain a transverse tensile load up to 1.2 MPa before an interface crack, which is very small compared to the transverse tensile strength, 27.7 MPa. This is consistent with a common observation that a Kevlar fiber-reinforced polymer matrix composite generally undergoes a much earlier interface debonding before an ultimate failure.

It is noticed that the three kinds of predictions arrive at the same longitudinal strength for each composite, i.e., 1137 MPa for the Kevlar fiber and 852 MPa for the E-glass fiber composites. Both of them correlate well with the experimental data, i.e., 1142 MPa for the Kevlar composite [53] and 817.5 MPa for the glass composite [52]. However, both of them have already undergone an interface crack ( $\hat{\sigma}_{00}^0 = 22.3$  MPa for the Kevlar and 725.4 MPa for the glass composites) before the longitudinal strength is attained. Both of the examples confirm that only a transverse tensile load carrying capacity is influenced by an interface crack.

## 9. Conclusion

Micromechanical failure and strength prediction of a UD composite is systematically described in this chapter. The internal stresses in the fiber and matrix must be calculated at first. Although various methods are available for this purpose, a thorough compassion study has shown that Bridging Model is the most potential owing to its simplicity with closed-form formulae, high accuracy, and the unique feature of consistency in the internal stress calculation. These stresses are homogenized quantities. They must be converted into true values before being used for a failure assessment against the original strength data of the fiber and matrix. Otherwise, a predicted strength of the composite may be far away from the experiment. The difference in the overall prediction accuracies between use of the homogenized

and the true stresses can be as large as more than five times. As the homogenized and the true stresses in the fiber are the same, the true stress determination for the matrix becomes essential. It has been demonstrated in the chapter that the true stresses of the matrix under any load condition are obtained by multiplying its homogenized counterparts with SCFs of the matrix in the composites. Such an SCF cannot be determined following a classical way. Instead, it must be defined as a line-averaged stress divided by a volume-averaged quantity. All of the SCFs subjected to various kinds of loading and with a perfect interface bonding have been presented in the chapter. It is known that an interface debonding only has a significant influence on the transverse tensile load carrying ability, and the transverse tensile SCF of the matrix after the interface debonding has also been obtained. The theory is equally well applicable to the failure and strength prediction of any other continuous fiber-reinforced composite, once it is subdivided into a combination of UD composites.

## Acknowledgements

Partial financial supports from the National Natural Science Foundation of China with grant numbers of 11832014 and 11472192 are greatly acknowledged.

## Appendix A. Formulae of micromechanics models

### A.1 Eshelby's method

The stiffness tensor of the composite by this method is given by [15]

$$[K_{ij}] = [S_{ij}]^{-1} = [K_{ij}^m] + V_f \left( [K_{ij}^f] - [K_{ij}^m] \right) \left\{ [I] + [L_{ij}] [S_{ij}^m] \left( [K_{ij}^f] - [K_{ij}^m] \right) \right\}^{-1}, \quad (\text{A.1})$$

$[K_{ij}^f]$  and  $[K_{ij}^m]$  are the stiffness tensors of the fiber and matrix, respectively, and  $[L_{ij}]$  is the Eshelby's tensor reading [16]

$$[L_{ij}] = \begin{bmatrix} 0 & 0 & 0 & 0 & 0 & 0 \\ L_{2211} & L_{2222} & L_{2233} & 0 & 0 & 0 \\ L_{3311} & L_{3322} & L_{3333} & 0 & 0 & 0 \\ 0 & 0 & 0 & 2L_{2323} & 0 & 0 \\ 0 & 0 & 0 & 0 & 2L_{1313} & 0 \\ 0 & 0 & 0 & 0 & 0 & 2L_{1212} \end{bmatrix}, \quad (\text{A.2})$$

$$L_{2211} = L_{3311} = \frac{\nu^m}{2(1-\nu^m)}, L_{2222} = L_{3333} = \frac{1}{2(1-\nu^m)} \left[ \frac{3}{4} + \frac{(1-2\nu^m)}{2} \right],$$

$$L_{1212} = L_{1313} = 1/4,$$

$$L_{2233} = L_{3322} = \frac{1}{2(1-\nu^m)} \left[ \frac{1}{4} - \frac{(1-2\nu^m)}{2} \right], L_{2323} = \frac{1}{2(1-\nu^m)} \left[ \frac{1}{4} + \frac{(1-2\nu^m)}{2} \right]. \quad (\text{A.3})$$

$\nu^m$  is Poisson's ratio of the matrix.

## A.2 Mori-Tanaka method

Non-zero bridging tensor elements of Mori-Tanaka method are given below [54]:

$$A_{11} = \frac{E^m}{E_{11}^f} \left( 1 + \frac{\nu^m (\nu^m - \nu_{12}^f)}{(1 + \nu^m)(1 - \nu^m)} \right), \quad (\text{A.4})$$

$$A_{12} = \frac{E^m}{E_{22}^f} \frac{\nu^m (1 - \nu_{23}^f)}{2(1 + \nu^m)(1 - \nu^m)} - \frac{E^m}{E_{11}^f} \frac{\nu_{12}^f}{(1 + \nu^m)(1 - \nu^m)} + \frac{\nu^m}{2(1 - \nu^m)} = A_{13}, \quad (\text{A.5})$$

$$A_{21} = \frac{E^m}{E_{11}^f} \frac{\nu^m - \nu_{12}^f}{2(1 + \nu^m)(1 - \nu^m)} = A_{31}, \quad (\text{A.6})$$

$$A_{22} = \frac{E^m}{E_{22}^f} \frac{(\nu_{23}^f - 3)}{8(\nu^m - 1)(\nu^m + 1)} + \frac{E^m}{E_{11}^f} \frac{\nu_{12}^f \nu^m}{2(\nu^m - 1)(\nu^m + 1)} + \frac{(\nu^m + 1)(4\nu^m - 5)}{8(\nu^m - 1)(\nu^m + 1)} = A_{33}, \quad (\text{A.7})$$

$$A_{32} = \frac{E^m}{E_{22}^f} \frac{(3\nu_{23}^f - 1)}{8(\nu^m - 1)(\nu^m + 1)} + \frac{E^m}{E_{11}^f} \frac{\nu_{12}^f \nu^m}{2(\nu^m - 1)(\nu^m + 1)} + \frac{(\nu^m + 1)(1 - 4\nu^m)}{8(\nu^m - 1)(\nu^m + 1)} = A_{23}, \quad (\text{A.8})$$

$$A_{44} = \frac{G^m}{G_{23}^f} \frac{1}{4(1 - \nu^m)} + \frac{(3 - 4\nu^m)}{4(1 - \nu^m)}, \quad (\text{A.9})$$

$$A_{55} = \frac{G^m + G_{12}^f}{2G_{12}^f} = A_{66}. \quad (\text{A.10})$$

$G_{23}^f$  is the fiber transverse shear modulus.

## A.3 Rule of mixture model

By this model, five elastic moduli of the composite are obtained as [19]

$$E_{11} = V_f E_{11}^f + V_m E^m, \quad (\text{A.11})$$

$$\nu_{12} = V_f \nu_{12}^f + V_m \nu^m, \quad (\text{A.12})$$

$$E_{22} = \frac{E^m}{1 - V_f \left( 1 - E^m / E_{22}^f \right)}, \quad (\text{A.13})$$

$$G_{12} = G_{13} = \frac{G^m}{1 - V_f \left( 1 - G^m / G_{12}^f \right)}, \quad (\text{A.14})$$

$$G_{23} = \frac{G^m}{1 - V_f \left( 1 - G^m / G_{23}^f \right)}. \quad (\text{A.15})$$

## A.4 Chamis model

By simply replacing  $V_f$  in Eqs. (A.13)–(A.15) with  $\sqrt{V_f}$ , respectively, one obtains the Chamis model's formulae [20].

### A.5 Modified rule of mixture model

Formulae for  $E_{11}$  and  $\nu_{12}$  are the same as Eqs. (A.11) and (A.12). The modified formulae for the other three moduli are [19]

$$E_{22} = \frac{4\eta_{22}G_{23}}{\eta_{22} + mG_{23}}, m = 1 + \frac{4\eta_{22}\nu_{12}^2}{E_{11}}, \frac{1}{\eta_{22}} = \frac{1}{V_f + \eta_k V_m} \left( \frac{V_f}{\Lambda_{22}^f} + \frac{V_m \eta_k}{\Lambda^m} \right), \quad (\text{A.16})$$

$$\frac{1}{G_{12}} = \frac{1}{V_f + \eta_{12} V_m} \left( \frac{V_f}{G_{12}^f} + \frac{V_m \eta_{12}}{G^m} \right), \eta_{12} = \frac{1}{2} \left( 1 + \frac{G^m}{G_{12}^f} \right), \quad (\text{A.17})$$

$$\frac{1}{G_{23}} = \frac{1}{V_f + \eta_{23} V_m} \left( \frac{V_f}{G_{23}^f} + \frac{V_m \eta_{23}}{G^m} \right), \eta_{23} = \frac{1}{4(1 - \nu^m)} \left( 3 - 4\nu^m + \frac{G^m}{G_{23}^f} \right), \quad (\text{A.18})$$

$$\eta_k = \frac{1}{2(1 - \nu^m)} \left( 1 + \frac{\Lambda^m}{\Lambda_{22}^f} \right), \quad (\text{A.19})$$

$$\Lambda_{22}^f = 0.5(K_{22}^f + K_{23}^f), \Lambda^m = 0.5(K_{22}^m + K_{23}^m). \quad (\text{A.20})$$

$K_{ij}^f$  and  $K_{ij}^m$  are the stiffness elements of the fiber and matrix.

### A.6 Halpin-Tsai formulae

$$E_{22} = \frac{4\Lambda_L G_{23}}{\Lambda_L + mG_{23}}, m = 1 + \frac{4\Lambda_L \nu_{12}^2}{E_{11}}, \frac{\Lambda_L}{\Lambda^m} = \frac{1 + (1 - 2\nu^m)\eta V_f}{1 - \eta V_f}, \quad (\text{A.21})$$

$$\frac{1}{G_{12}} = \frac{1}{V_f + \eta_{12} V_m} \left( \frac{V_f}{G_{12}^f} + \frac{V_m \eta_{12}}{G^m} \right), \eta_{12} = \frac{1}{2} \left( 1 + \frac{G^m}{G_{12}^f} \right), \quad (\text{A.22})$$

$$\frac{1}{G_{23}} = \frac{1}{V_f + \eta_{23} V_m} \left( \frac{V_f}{G_{23}^f} + \frac{V_m \eta_{23}}{G^m} \right), \eta_{23} = \frac{1}{4(1 - \nu^m)} \left( 3 - 4\nu^m + \frac{G^m}{G_{23}^f} \right), \quad (\text{A.23})$$

$$\eta = \frac{\Lambda_{22}^f / \Lambda^m - 1}{\Lambda_{22}^f / \Lambda^m + 1 - 2\nu^m}. \quad (\text{A.24})$$

It is noted that the formulae for  $E_{11}$  and  $\nu_{12}$  are the same as Eqs. (A.11) and (A.12), respectively [21].

### A.7 Hill-Hashin-Christensen-Lo model

$$E_{11} = V_f E_{11}^f + V_m E^m + \frac{4(\nu_{12}^f - \nu^m)^2 V_f (1 - V_f)}{\frac{V_f}{\Lambda^m} + \frac{1 - V_f}{\Lambda_{22}^f} + \frac{1}{G^m}}, \quad (\text{A.25})$$

$$\nu_{12} = V_f \nu_{12}^f + V_m \nu^m + \frac{(\nu_{12}^f - \nu^m) V_f (1 - V_f)}{\frac{V_f}{\Lambda^m} + \frac{1 - V_f}{\Lambda_{22}^f} + \frac{1}{G^m}} \left( \frac{1}{\Lambda^m} - \frac{1}{\Lambda_{22}^f} \right), \quad (\text{A.26})$$

$$E_{22} = \frac{2}{0.5/K_T + 0.5/G_{23} + 2\nu_{12}^2/E_{11}}, \quad (\text{A.27})$$

$$G_{12} = G^m \frac{(G_{12}^f + G^m) + V_f(G_{12}^f - G^m)}{(G_{12}^f + G^m) - V_f(G_{12}^f - G^m)}, \quad (\text{A.28})$$

$$K_T = K^m + \frac{V_f}{\frac{1}{\Lambda_{22}^f - \Lambda^m} + \frac{1 - V_f}{\Lambda^m + G^m}}, \quad (\text{A.29})$$

$$A_1 \left( \frac{G_{23}}{G_m} \right)^2 + 2B \left( \frac{G_{23}}{G_m} \right) + C_1 = 0, \quad (\text{A.30})$$

$$A_1 = 3V_f V_m^2 \left( \frac{G^f}{G^m} - 1 \right) \left( \frac{G^f}{G^m} + \eta_f \right) + \left[ \frac{G^f}{G^m} \eta_m + \eta_f \eta_m - \left( \frac{G^f}{G^m} \eta_m - \eta_f \right) V_f^3 \right] \left[ V_f \eta_m \left( \frac{G^f}{G^m} - 1 \right) - \left( \frac{G^f}{G^m} \eta_m + 1 \right) \right], \quad (\text{A.31})$$

$$B_1 = -3V_f V_m^2 \left( \frac{G^f}{G^m} - 1 \right) \left( \frac{G^f}{G^m} + \eta_f \right) + \frac{1}{2} \left[ \frac{G^f}{G^m} \eta_m + \left( \frac{G^f}{G^m} - 1 \right) V_f + 1 \right] \left[ (\eta_m - 1) \left( \frac{G^f}{G^m} + \eta_f \right) - 2 \left( \frac{G^f}{G^m} \eta_m - \eta_f \right) V_f^3 \right] + \frac{V_f}{2} (\eta_m + 1) \left( \frac{G^f}{G^m} - 1 \right) \left[ \frac{G^f}{G^m} + \eta_f + \left( \frac{G^f}{G^m} \eta_m - \eta_f \right) V_f^3 \right], \quad (\text{A.32})$$

$$C_1 = 3V_f V_m^2 \left( \frac{G^f}{G^m} - 1 \right) \left( \frac{G^f}{G^m} + \eta_f \right) + \left[ \frac{G^f}{G^m} \eta_m + V_f \left( \frac{G^f}{G^m} - 1 \right) + 1 \right] \left[ \frac{G^f}{G^m} + \eta_f + \left( \frac{G^f}{G^m} \eta_m - \eta_f \right) V_f^3 \right], \quad (\text{A.33})$$

$$\eta_f = 3 - 4\nu_{23}^f, \eta_m = 3 - 4\nu_m. \quad (\text{A.34})$$

Eq. (A.30) is applicable only to composites with an isotropic fiber reinforcement [22].

## A.8 Self-consistent model

The self-consistent formulae are represented as follows [15]:

$$[K_{ij}] = [K_{ij}^m] + V_f \left( [K_{ij}^f] - [K_{ij}^m] \right) [M_{ij}^f] \quad (\text{A.35})$$

$$[M_{ij}^f] = \left\{ [I] + [\tilde{L}_{ij}] [S_{ij}] \left( [K_{ij}^f] - [K_{ij}] \right) \right\}^{-1} \quad (\text{A.36})$$

$$[\tilde{L}_{ij}] = \left( [S_{ij}] [\tilde{A}_{ij}] [K_{ij}^f] - [I] \right) \left( [K_{ij}^f] - [K_{ij}] \right)^{-1} [K_{ij}] \quad (\text{A.37})$$

where  $[\tilde{A}_{ij}]$  is the bridging tensor correlating the homogenized stresses of the composite with those of the fiber in a concentric cylinder assemblage (CCA)

model, i.e., a two-phase CCA model, through  $\{\sigma_i\} = [\tilde{A}_{ij}]\{\sigma_j^f\}$ , whose non-zero elements are given by [54]

$$\tilde{A}_{11} = \frac{E_{11}(E_{11} - E_{22}\nu_{12}^f\nu_{12})}{E_{11}^f[E_{11} - E_{22}(\nu_{12})^2]}, \quad (\text{A.38})$$

$$\tilde{A}_{12} = \tilde{A}_{13} = \frac{E_{11}\{E_{11}^f E_{22}(1 - \nu_{23}^f)\nu_{12} + E_{22}^f[-2E_{11}\nu_{12}^f + E_{11}^f\nu_{12}(1 + \nu_{23})]\}}{2E_{11}^f E_{22}^f[E_{11} - E_{22}(\nu_{12})^2]}, \quad (\text{A.39})$$

$$\tilde{A}_{21} = \tilde{A}_{31} = \frac{E_{11}E_{22}(\nu_{12} - \nu_{12}^f)}{2E_{11}^f[E_{11} - E_{22}(\nu_{12})^2]}, \quad (\text{A.40})$$

$$\tilde{A}_{22} = \tilde{A}_{33} = \frac{E_{11}[E_{22}^f(5 + \nu_{23}) + E_{22}(3 - \nu_{23}^f)]}{8E_{22}^f[E_{11} - E_{22}(\nu_{12})^2]} - \frac{E_{22}\nu_{12}(E_{11}\nu_{12}^f + E_{11}^f\nu_{12})}{2E_{11}^f[E_{11} - E_{22}(\nu_{12})^2]}, \quad (\text{A.41})$$

$$\tilde{A}_{23} = \tilde{A}_{32} = \frac{E_{11}[E_{22}(1 - 3\nu_{23}^f) + E_{22}^f(3\nu_{23} - 1)]}{8E_{22}^f[E_{11} - E_{22}(\nu_{12})^2]} + \frac{E_{22}\nu_{12}(E_{11}^f\nu_{12} - E_{11}\nu_{12}^f)}{2E_{11}^f[E_{11} - E_{22}(\nu_{12})^2]}, \quad (\text{A.42})$$

$$\tilde{A}_{44} = \frac{(1 + \nu_{23}^f)\{-8E_{22}G_{23}^f(\nu_{12})^2 + E_{11}[E_{22} + 2G_{23}^f(3 - \nu_{23})]\}}{4E_{22}^f[E_{11} - E_{22}(\nu_{12})^2]}, \quad (\text{A.43})$$

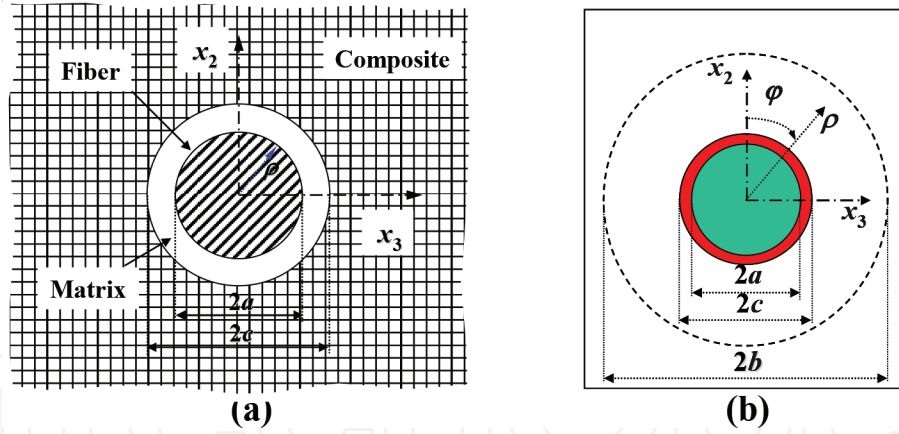
$$\tilde{A}_{55} = \tilde{A}_{66} = \frac{G_{12}^f + G_{12}}{2G_{12}^f}. \quad (\text{A.44})$$

The self-consistent model is implicit, and an iteration has to be carried out to determine the five effective elastic moduli,  $E_{11}$ ,  $E_{22}$ ,  $G_{12}$ ,  $\nu_{12}$ , and  $\nu_{23}$ , of the composite.

## A.9 Generalized self-consistent model

Basic equations of the generalized self-consistent model are the same as Eqs. (A.35)–(A.37), except that the bridging tensor in Eq. (A.37),  $[\tilde{A}_{ij}]$ , correlating the stresses of the composite with those of the fiber is no longer obtained on a two-phase CCA model but on a three-phase CCA one shown in **Figure A.1**. In the latter case, however, generally non-explicit expressions exist for the bridging tensor elements  $\tilde{A}_{ij}$ . Solution for the resulting linear algebraic equations is necessary [54].

As pointed out in Ref. [54], a three-phase CCA model (**Figure A.1**) can be sufficiently well approximated with two step two-phase CCA ones. In the first step, the fiber and matrix phase constitutes a UD composite, whose effective elastic moduli,  $E_{11}^{eq}$ ,  $E_{22}^{eq}$ ,  $\nu_{12}^{eq}$ ,  $G_{12}^{eq}$ , and  $\nu_{23}^{eq}$ , can be obtained from Eq. (6) in which the bridging tensor  $[A_{ij}]$  is defined by Eqs. (A.4)–(A.10). Then, this UD composite is regarded as an equivalent fiber to embed into the composite. The resulting bridging tensor  $[A_{ij}^{eq}]$  correlating the stresses of the composite with those of the equivalent fiber is given by Eqs. (A.38)–(A.44), providing that  $E_{11}^f$ ,  $E_{22}^f$ ,  $\nu_{12}^f$ ,  $G_{12}^f$ , and  $\nu_{23}^f$  involved are replaced by  $E_{11}^{eq}$ ,  $E_{22}^{eq}$ ,  $\nu_{12}^{eq}$ ,  $G_{12}^{eq}$ , and  $\nu_{23}^{eq}$ , respectively.


**Figure A.1.**

(a) Schematic for generalized self-consistent method. (b) A three-phase CCA model (b $\rightarrow$ ) for the generalized self-consistent method.

From  $\{\sigma_i\} = [A_{ij}^{eq}] \{\sigma_j^{eq}\}$  and  $\{\sigma_i^f\} = (V_f[I] + V_m[A_{ij}])^{-1} \{\sigma_j^{eq}\}$ , it is obtained that

$$[\tilde{A}_{ij}] \approx [A_{ij}^{eq}] (V_f[I] + V_m[A_{ij}]). \quad (\text{A.45})$$

## A.10 Double inclusion method (DIM)

This method [4] has been incorporated into a commercial software, Digimat [40], for composites. As any prediction by this method is performed with Digimat, the formulae of the method are omitted.

## Appendix B. Mechanical property data tables

	E-glass LY556	E-glass MY750	AS4 3501-6	T300 BSL914C	IM7 8511-7	T300 PR319	AS epoxy	S2-glass epoxy	G400-800 5260
$E_{11}^f$ (GPa)	80	74	225	230	276	230	231	87	290
$E_{22}^f$ (GPa)	80	74	15	15	19	15	15	87	19
$\nu_{12}^f$	0.2	0.2	0.2	0.2	0.2	0.2	0.2	0.2	0.2
$G_{12}^f$ (GPa)	33.33	30.8	15	15	27	15	15	36.3	27
$\nu_{23}^f$	0.2	0.2	0.07	0.07	0.36	0.07	0.07	0.2	0.357
$\sigma_{u,t}^f$ (MPa)	2150	2150	3350	2500	5180	2500	3500	2850	5860
$\sigma_{u,c}^f$ (MPa)	1450	1450	2500	2000	3200	2000	3000	2450	3200
$E^m$ (GPa)	3.35	3.35	4.2	4	4.08	0.95	3.2	3.2	3.45
$\nu^m$	0.35	0.35	0.34	0.35	0.38	0.35	0.35	0.35	0.35
$\sigma_{u,t}^m$ (MPa)	80	80	69	75	99	70	85	73	70
$\sigma_{u,c}^m$ (MPa)	120	120	250	150	130	130	120	120	130
$\sigma_{u,s}^m$ (MPa)	54	54	50	70	57	41	50	52	57
$V_f$	0.62	0.6	0.6	0.6	0.6	0.6	0.6	0.6	0.6

**Table B1.**

Mechanical properties of the fibers and matrices of the nine UD composites used in WWFEs [25–27].

	E-glass LY556	E-glass MY750	AS4 3501-6	T300 BSL914C	IM7 8511-7	T300 PR319	AS epoxy	S2-glass epoxy	G400-800 5260
$E_{11}$ (GPa)	53.5	45.6	126	138	165	129	140	52	173
$E_{22}$ (GPa)	17.7	16.2	11	11	8.4	5.6	10	19	10
$\nu_{12}$	0.278	0.278	0.28	0.28	0.34	0.318	0.3	0.3	0.33
$G_{12}$ (GPa)	5.83	5.83	6.6	5.5	5.6	1.33	6	6.7	6.94
$G_{23}$ (GPa)	6.32	5.79	3.93	3.93	2.8	1.86	3.35	6.7	3.56
$\sigma_{11}^{u,t}$ (MPa)	1140	1280	1950	1500	2560	1378	1990	1700	2750
$\sigma_{11}^{u,c}$ (MPa)	570	800	1480	900	1590	950	1500	1150	1700
$\sigma_{22}^{u,t}$ (MPa)	35	40	48	27	73	40	38	63	75
$\sigma_{22}^{u,c}$ (MPa)	114	145	200	200	185	125	150	180	210
$\sigma_{12}^u$ (MPa)	72	73	79	80	90	97	70	72	90
$\sigma_{23}^u$ (MPa)	50	50	55	-	57	45	50	40	57

**Table B2.**  
*Mechanical properties of the nine UD composites used in WWFEs [25–27].*

	E-glass LY556	E-glass MY750	AS4 3501-6	T300 BSL914C	IM7 8511-7	T300 PR319	AS epoxy	S2-glass epoxy	G400-800 5260
<b>By Eshelby's method</b>									
$E_{11}$ (GPa)	50.81	45.68	136.61	139.51	167.07	138.36	139.81	53.42	175.31
$E_{22}$ (GPa)	7.15	7.01	7.30	7.08	7.73	1.98	5.91	6.76	6.52
$\nu_{12}$	0.28	0.28	0.27	0.27	0.29	0.28	0.27	0.28	0.28
$G_{12}$ (GPa)	2.67	2.61	3.09	2.94	3.07	0.76	2.40	2.52	2.68
$G_{23}$ (GPa)	2.42	2.37	2.60	2.49	2.50	0.67	2.05	2.28	2.19
<b>By Bridging Model</b>									
$E_{11}$ (GPa)	50.9	45.7	136.7	139.6	167.2	138.4	139.9	53.5	175.4
$E_{22}$ (GPa)	18.1	16.8	9.7	9.6	11.2	4.41	8.7	16.9	10.2
$\nu_{12}$	0.257	0.26	0.256	0.26	0.272	0.26	0.26	0.26	0.26
$G_{12}$ (GPa)	6.28	5.84	5.54	5.35	6.46	1.82	4.64	5.81	5.8
$G_{23}$ (GPa)	6.24	5.8	3.76	3.66	3.76	1.55	3.29	5.77	3.51
<b>By Mori-Tanaka's method</b>									
$E_{11}$ (GPa)	50.9	45.76	136.7	139.6	167.3	138.4	139.9	53.5	175.4
$E_{22}$ (GPa)	11.7	11.02	8.757	8.573	9.665	3.02	7.481	10.78	8.473
$\nu_{12}$	0.249	0.252	0.26	0.257	0.267	0.252	0.256	0.252	0.254
$G_{12}$ (GPa)	4.60	4.32	4.53	4.35	4.92	1.30	3.67	4.23	4.36
$G_{23}$ (GPa)	4.06	3.83	3.32	3.21	3.23	1.06	2.77	3.72	2.92
<b>By rule of mixture method</b>									
$E_{11}$ (GPa)	50.87	45.74	136.7	139.6	167.2	138.38	139.88	53.5	175.4
$E_{22}$ (GPa)	8.252	7.84	7.394	7.14	7.715	2.169	6.061	7.5817	6.779
$\nu_{12}$	0.257	0.26	0.256	0.26	0.272	0.26	0.26	0.26	0.26

	E-glass LY556	E-glass MY750	AS4 3501-6	T300 BSL914C	IM7 8511-7	T300 PR319	AS epoxy	S2-glass epoxy	G400-800 5260
$G_{12}$ (GPa)	3.08	2.92	3.39	3.23	3.42	0.85	2.65	2.82	2.99
$G_{23}$ (GPa)	3.08	2.92	2.93	2.81	2.81	0.82	2.36	2.82	2.51
<b>By Chamis method</b>									
$E_{11}$ (GPa)	50.87	45.74	136.7	139.6	167.2	138.38	139.88	53.5	175.4
$E_{22}$ (GPa)	13.64	12.86	9.496	9.26	10.415	3.461	8.192	12.604	9.425
$\nu_{12}$	0.257	0.26	0.256	0.26	0.272	0.272	0.26	0.26	0.26
$G_{12}$ (GPa)	5.13	4.83	5.12	4.91	5.52	1.45	4.14	4.73	4.88
$G_{23}$ (GPa)	5.13	4.83	3.93	3.81	3.80	1.33	3.33	4.73	3.49
<b>By modified rule of mixture method</b>									
$E_{11}$ (GPa)	50.87	45.74	136.7	139.6	167.2	138.38	139.88	53.5	175.4
$E_{22}$ (GPa)	11.61	10.93	8.65	8.46	9.53	2.98	7.37	10.71	8.35
$\nu_{12}$	0.257	0.26	0.256	0.26	0.272	0.272	0.26	0.26	0.26
$G_{12}$ (GPa)	4.60	4.32	4.54	4.35	4.92	1.29	3.67	4.23	4.35
$G_{23}$ (GPa)	4.06	3.82	3.32	3.21	3.23	1.06	2.77	3.73	2.91
<b>By Halpin-Tsai formulae</b>									
$E_{11}$ (GPa)	50.87	45.74	136.7	139.6	167.2	138.38	139.88	53.5	175.4
$E_{22}$ (GPa)	11.69	11.0	8.76	8.57	9.66	3.02	7.48	10.77	8.47
$\nu_{12}$	0.257	0.26	0.256	0.26	0.272	0.272	0.26	0.26	0.26
$G_{12}$ (GPa)	4.60	4.32	4.54	4.35	4.92	1.29	3.67	4.23	4.35
$G_{23}$ (GPa)	4.06	3.82	3.32	3.21	3.23	1.06	2.77	3.73	2.91
<b>By Hill-Hashin-Christensen-Lo method</b>									
$E_{11}$ (GPa)	50.9	45.8	136.7	139.6	167.3	138.4	139.9	53.5	175.4

	E-glass LY556	E-glass MY750	AS4 3501-6	T300 BSL914C	IM7 8511-7	T300 PR319	AS epoxy	S2-glass epoxy	G400-800 5260
$E_{22}$ (GPa)	12.9	12.0	—	—	—	—	—	11.85	—
$\nu_{12}$	0.249	0.252	0.253	0.257	0.267	0.252	0.256	0.25	0.25
$G_{12}$ (GPa)	4.6	4.32	4.54	4.35	4.92	1.29	3.67	4.23	4.35
$G_{23}$ (GPa)	4.65	4.33	—	—	—	—	—	4.25	—
<b>By self-consistent method</b>									
$E_{11}$ (GPa)	50.94	45.81	136.72	139.65	167.31	138.40	139.92	53.55	175.43
$E_{22}$ (GPa)	18.91	16.80	9.14	8.99	10.37	4.19	8.06	17.39	9.33
$\nu_{12}$	0.231	0.235	0.250	0.254	0.262	0.238	0.251	0.233	0.247
$G_{12}$ (GPa)	11.34	9.80	6.37	6.25	9.36	4.18	5.82	10.94	8.98
$G_{23}$ (GPa)	6.96	6.15	3.53	3.43	3.52	1.55	3.06	6.36	3.25
<b>By generalized self-consistent method</b>									
$E_{11}$ (GPa)	50.9	45.8	136.7	139.6	167.3	138.4	139.9	53.5	175.4
$E_{22}$ (GPa)	12.87	12.03	8.93	8.77	10.1	3.27	7.72	11.8	8.85
$\nu_{12}$	0.249	0.252	0.253	0.257	0.27	0.25	0.256	0.25	0.254
$G_{12}$ (GPa)	4.6	4.32	4.54	4.3	4.9	1.2	3.6	4.2	4.35
$G_{23}$ (GPa)	4.65	4.33	3.42	3.32	3.42	1.19	2.9	4.25	3.09
<b>By double-inclusion method (Digimat [40])</b>									
$E_{11}$ (GPa)	50.9	47.2	141.1	144.2	172.8	143	144.5	55.2	181.2
$E_{22}$ (GPa)	16.2	15.9	9.35	9.2	10.5	4.11	8.26	16.1	9.48
$\nu_{12}$	0.234	0.234	0.248	0.252	0.257	0.238	0.249	0.234	0.244
$G_{12}$ (GPa)	6.73	6.585	5.8	5.63	7.12	2.13	5	6.65	6.46

	E-glass LY556	E-glass MY750	AS4 3501-6	T300 BSL914C	IM7 8511-7	T300 PR319	AS epoxy	S2-glass epoxy	G400-800 5260
$G_{23}$ (GPa)	5.78	5.67	3.64	3.54	3.55	1.51	3.16	5.7	3.28
<b>By FE-square fiber array</b>									
$E_{11}$ (GPa)	50.9	45.8	136.7	139.6	167.3	138.4	139.9	53.5	175.4
$E_{22}$ (GPa)	16.26	14.9	9.54	9.42	10.88	3.98	8.45	14.86	9.63
$\nu_{12}$	0.246	0.25	0.252	0.256	0.266	0.25	0.255	0.249	0.252
$G_{12}$ (GPa)	4.96	4.58	4.68	4.5	5.15	1.38	3.82	4.5	4.57
$G_{23}$ (GPa)	6.49	5.89	3.79	3.71	3.79	1.58	3.32	5.89	3.47
<b>By FE-hexagonal fiber array</b>									
$E_{11}$ (GPa)	50.89	45.77	136.70	139.56	167.26	138.38	139.90	53.50	175.37
$E_{22}$ (GPa)	12.60	11.72	8.89	8.72	9.89	3.19	7.66	11.51	8.68
$\nu_{12}$	0.249	0.251	0.253	0.255	0.267	0.259	0.256	0.251	0.252
$G_{12}$ (GPa)	4.62	4.32	4.54	4.35	4.91	1.30	3.67	4.22	4.35
$G_{23}$ (GPa)	3.03	4.18	3.40	3.29	3.32	1.14	2.86	4.07	3.01
<b>By FE-square diagonal fiber array</b>									
$E_{11}$ (GPa)	50.89	45.77	136.71	139.56	167.30	138.42	139.88	53.51	175.43
$E_{22}$ (GPa)	10.40	9.85	8.30	8.09	9.03	2.71	7.12	9.60	7.92
$\nu_{12}$	0.248	0.250	0.251	0.255	0.264	0.251	0.260	0.250	0.255
$G_{12}$ (GPa)	4.87	4.56	4.68	4.50	5.16	1.38	3.82	4.48	4.58
$G_{23}$ (GPa)	2.59	3.25	3.06	2.94	2.95	0.90	2.50	3.15	2.65
<b>By FE-random fiber array</b>									
$E_{11}$ (GPa)	50.90	45.77	136.71	139.37	167.27	138.37	139.90	53.51	175.41
$E_{22}$ (GPa)	13.76	12.79	8.92	8.76	9.97	3.43	7.73	12.77	8.84

	E-glass LY556	E-glass MY750	AS4 3501-6	T300 BSL914C	IM7 8511-7	T300 PR319	AS epoxy	S2-glass epoxy	G400-800 5260
$\nu_{12}$	0.241	0.245	0.248	0.255	0.263	0.241	0.252	0.243	0.250
$G_{12}$ (GPa)	4.58	4.29	4.42	4.33	4.69	1.29	3.60	4.21	4.29
$G_{23}$ (GPa)	5.08	4.74	3.48	3.53	3.43	1.28	2.97	4.69	3.12

**Table B3.**  
*Predicted elastic moduli of the nine UD composites by different models.*

	E-glass LY556	E-glass MY750	AS4 3501-6	T300 BSL914C	IM7 8511-7	T300 PR319	AS epoxy	S2-glass epoxy	G400-800 5260
<b>Eshelby's method</b>									
$\lambda_1$	1.577	1.623	1.648	1.650	1.654	1.663	1.653	1.631	1.655
$\lambda_2$	1.370	1.322	1.204	1.205	1.247	1.308	1.234	1.324	1.270
$\lambda_3$	1.301	1.257	1.220	1.218	1.201	1.255	1.228	1.259	1.225
$\lambda_4$	1.169	1.131	1.123	1.124	1.130	1.133	1.126	1.132	1.130
<b>Bridging Model</b>									
$\lambda_1$	1.573	1.618	1.646	1.648	1.650	1.662	1.651	1.627	1.654
$\lambda_2$	0.442	0.453	0.621	0.612	0.577	0.467	0.576	0.446	0.554
$\lambda_3$	0.442	0.453	0.621	0.612	0.577	0.467	0.576	0.446	0.554
$\lambda_4$	0.438	0.449	0.498	0.494	0.460	0.436	0.479	0.443	0.454
<b>Mori-Tanaka's method</b>									
$\lambda_1$	1.571	1.616	1.647	1.647	1.650	1.662	1.651	1.625	1.653
$\lambda_2$	0.793	0.801	0.868	0.867	0.855	0.807	0.852	0.797	0.841
$\lambda_3$	0.734	0.739	0.800	0.793	0.782	0.743	0.780	0.738	0.782
$\lambda_4$	0.635	0.644	0.674	0.670	0.650	0.636	0.661	0.640	0.647
<b>Rule of mixture method</b>									
$\lambda_1$	1.573	1.618	1.646	1.648	1.650	1.662	1.651	1.627	1.654
$\lambda_2$	1.304	1.303	1.661	1.755	1.725	1.352	1.576	1.304	1.418
$\lambda_3$	1.001	1.002	1.000	1.001	1.000	0.999	1.000	1.000	0.998
$\lambda_4$	1.000	1.001	1.000	1.000	1.000	1.000	1.000	1.000	1.000
<b>Chamis method</b>									
$\lambda_1$	1.573	1.618	1.646	1.648	1.650	1.662	1.651	1.627	1.654

	E-glass LY556	E-glass MY750	AS4 3501-6	T300 BSL914C	IM7 8511-7	T300 PR319	AS epoxy	S2-glass epoxy	G400-800 5260
$\lambda_2$	0.720	0.724	0.925	0.977	0.964	0.761	0.882	0.726	0.796
$\lambda_3$	0.560	0.564	0.564	0.564	0.564	0.563	0.564	0.564	0.562
$\lambda_4$	0.560	0.564	0.563	0.563	0.564	0.564	0.563	0.564	0.564
<b>Modified rule of mixture method</b>									
$\lambda_1$	1.573	1.618	1.646	1.648	1.650	1.662	1.651	1.627	1.654
$\lambda_2$	0.808	0.813	0.957	0.966	0.934	0.840	0.933	0.811	0.890
$\lambda_3$	0.734	0.741	0.800	0.793	0.780	0.742	0.779	0.737	0.785
$\lambda_4$	0.635	0.643	0.672	0.671	0.650	0.638	0.662	0.640	0.648
<b>Halpin-Tsai formulae</b>									
$\lambda_1$	1.573	1.618	1.646	1.648	1.650	1.662	1.651	1.627	1.654
$\lambda_2$	0.794	0.800	0.867	0.870	0.860	0.809	0.856	0.800	0.839
$\lambda_3$	0.734	0.741	0.800	0.793	0.780	0.742	0.779	0.737	0.785
$\lambda_4$	0.635	0.643	0.672	0.671	0.650	0.638	0.662	0.640	0.648
<b>Hill-Hashin-Christensen-Lo method</b>									
$\lambda_1$	1.571	1.616	—	—	—	—	—	1.625	—
$\lambda_2$	0.727	0.755	—	—	—	—	—	0.745	—
$\lambda_3$	0.636	0.642	—	—	—	—	—	0.636	—
$\lambda_4$	0.635	0.643	—	—	—	—	—	0.640	—
<b>Self-consistent method</b>									
$\lambda_1$	1.567	1.612	1.645	1.646	1.649	1.662	1.650	1.622	1.653
$\lambda_2$	0.459	0.496	0.806	0.795	0.764	0.549	0.755	0.471	0.713

	E-glass LY556	E-glass MY750	AS4 3501-6	T300 BSL914C	IM7 8511-7	T300 PR319	AS epoxy	S2-glass epoxy	G400-800 5260
$\lambda_3$	0.385	0.420	0.710	0.699	0.661	0.465	0.657	0.396	0.644
$\lambda_4$	0.197	0.224	0.395	0.382	0.272	0.155	0.338	0.195	0.250
<b>Generalized self-consistent method</b>									
$\lambda_1$	1.571	1.616	1.646	1.647	1.650	1.662	1.651	1.625	1.653
$\lambda_2$	0.792	0.799	0.870	0.867	0.854	0.809	0.857	0.798	0.839
$\lambda_3$	0.734	0.740	0.800	0.793	0.780	0.742	0.779	0.738	0.785
$\lambda_4$	0.635	0.643	0.673	0.671	0.650	0.638	0.662	0.640	0.648
<b>Double inclusion method (Digimat)</b>									
$\lambda_1$	1.568	1.617	1.647	1.648	1.650	1.662	1.652	1.626	1.654
$\lambda_2$	0.543	0.517	0.766	0.758	0.729	0.559	0.721	0.502	0.679
$\lambda_3$	0.485	0.465	0.666	0.657	0.649	0.481	0.620	0.453	0.633
$\lambda_4$	0.402	0.386	0.463	0.456	0.404	0.363	0.429	0.376	0.396
<b>FE-square fiber array</b>									
$\lambda_1$	1.570	1.616	1.645	1.647	1.649	1.662	1.651	1.625	1.653
$\lambda_2$	0.616	0.635	0.773	0.769	0.744	0.650	0.735	0.630	0.721
$\lambda_3$	0.421	0.444	0.612	0.596	0.566	0.454	0.565	0.436	0.568
$\lambda_4$	0.582	0.600	0.643	0.639	0.614	0.593	0.628	0.596	0.611
<b>FE-hexagonal fiber array</b>									
$\lambda_1$	1.571	1.616	1.646	1.646	1.650	1.662	1.651	1.625	1.653
$\lambda_2$	0.295	0.766	0.853	0.850	0.825	0.775	0.828	0.760	0.815
$\lambda_3$	1.019	0.669	0.765	0.756	0.741	0.677	0.737	0.667	0.742
$\lambda_4$	0.633	0.643	0.673	0.671	0.651	0.636	0.662	0.641	0.647

	E-glass LY556	E-glass MY750	AS4 3501-6	T300 BSL914C	IM7 8511-7	T300 PR319	AS epoxy	S2-glass epoxy	G400-800 5260
<b>FE- FE-square diagonal fiber array</b>									
$\lambda_1$	1.571	1.616	1.645	1.646	1.649	1.662	1.651	1.625	1.653
$\lambda_2$	0.454	0.856	0.932	0.928	0.921	0.864	0.809	0.856	0.898
$\lambda_3$	1.210	0.890	0.928	0.926	0.919	0.893	0.918	0.887	0.916
$\lambda_4$	0.594	0.604	0.643	0.640	0.613	0.593	0.628	0.599	0.609
<b>FE-random fiber array</b>									
$\lambda_1$	1.570	1.615	1.645	1.647	1.649	1.662	1.651	1.625	1.653
$\lambda_2$	0.660	0.676	0.830	0.826	0.802	0.694	0.798	0.662	0.777
$\lambda_3$	0.566	0.578	0.731	0.662	0.695	0.592	0.692	0.569	0.693
$\lambda_4$	0.611	0.621	0.606	0.601	0.634	0.609	0.650	0.615	0.629

**Table B4.**

The coefficients  $\lambda_i$ 's for the nine composites by different models.

IntechOpen

IntechOpen

### **Author details**

Zheng-Ming Huang  
School of Aerospace Engineering and Applied Mechanics, Tongji University,  
Shanghai, China

\*Address all correspondence to: [huangzm@tongji.edu.cn](mailto:huangzm@tongji.edu.cn)

### **IntechOpen**

---

© 2018 The Author(s). Licensee IntechOpen. This chapter is distributed under the terms of the Creative Commons Attribution License (<http://creativecommons.org/licenses/by/3.0>), which permits unrestricted use, distribution, and reproduction in any medium, provided the original work is properly cited. 

## References

- [1] Llorca J, González C, Molina-Aldareguía JM, Segurado J, Seltzer R, Sket F, et al. Multiscale modeling of composite materials: A roadmap towards virtual testing. *Advanced Materials*. 2011;**23**:5130-5147
- [2] Bogdanovich AE, Sierakowski RL. Composite materials and structures: Science, technology and applications—A compendium of books, review papers, and other sources of information. *Applied Mechanics Reviews*. 1999; **52**(12):351-366
- [3] Pindera MJ, Khatam H, Drago AS, Bansal Y. Micromechanics of spatially uniform heterogeneous media: A critical review and emerging approaches. *Composites, Part B*. 2009;**40**(5):349-378
- [4] Nemat-Nasser S, Hori M. *Micromechanics: Overall Properties of Heterogeneous Materials*. Amsterdam: Elsevier; 2013
- [5] Hinton MJ, Kaddour AS, Soden PD. *Failure Criteria in Fiber Reinforced Polymer Composites*. Amsterdam, The Netherlands: Elsevier; 2004
- [6] Eshelby JD. The determination of the elastic field of an ellipsoidal inclusion and related Problems. *Proceedings of the Royal Society*. 1957;**A240**:367-396
- [7] Chen T, Dvorak GJ, Benveniste Y. Stress fields in composites reinforced by coated cylindrically orthotropic fibers. *Mechanics of Materials*. 1990;**9**:17-32
- [8] Huang Z-M, Liu L. Predicting strength of fibrous laminates under triaxial loads only upon independently measured constituent properties. *International Journal of Mechanical Sciences*. 2014;**79**(1):105-129
- [9] Huang Z-M, Xin L-M. Stress concentration factor in matrix of a composite subjected to transverse compression. *International Journal of Applied Mechanics*. 2016;**8**(3): 1650034-1-1650034-165003418
- [10] Huang Z-M, Xin L-M. In situ strengths of matrix in a composite. *Acta Mechanica Sinica*. 2017;**33**(1): 120-131
- [11] Zhou Y, Huang Z-M, Liu L. Prediction of interfacial debonding in fiber-reinforced composite laminates. *Polymer Composites*. (Accepted for publication)
- [12] Ryan S, Wicklein M, Mouritz A, Riedel W, Schäfer F, Thoma K. Theoretical prediction of dynamic composite material properties for hypervelocity impact simulations. *International Journal of Impact Engineering*. 2009;**36**(7):899-912
- [13] Younes R, Hallal A, Fardoun F, Chehade FH. Comparative review study on elastic properties modeling for unidirectional composite materials. In: Hu N, editor. *Composites and Their Properties*. InTech; 2012. pp. 391-408. DOI: 10.5772/50362
- [14] Medikonda STA, Hamm R. A comparative study of the effect of representative volume cell (RVC) boundary conditions on the elastic properties of a micromechanics based unidirectional composite material model. *International Journal of Computational Materials*. 2017;**7**(2):51-71
- [15] Qu J, Cherkaoui M. *Fundamentals of Micromechanics of Solids*. New Jersey: John Wiley & Sons; 2006
- [16] Huang Z-M, Zhou Y-X. *Strength of Fibrous Composites*. Zhejiang Univ. New York: Press & Springer; 2011
- [17] Mori T, Tanaka K. Average stress in matrix and average energy of materials

with misfitting inclusion. *Acta Metallurgica*. 1973;**21**:571-574

[18] Benveniste Y. A new approach to the application of Mori-Tanaka's theory in composite materials. *Mechanics of Materials*. 1987;**6**(2):147-157

[19] Tsai SW, Hahn HT. *Introduction to Composite Materials*. Boca Roca: CRC Press; 1980

[20] Chamis CC. Mechanics of composite materials: Past, present and future. *Journal of Composites Technology and Research*. 1989;**11**(1):3-14

[21] Halpin JC, Kardos JL. The Halpin-Tsai equations: A review. *Polymer Engineering and Science*. 1976;**16**:344-352

[22] Swanson SR. *Introduction to Design and Analysis with Advanced Composite Materials*. New Jersey: Prentice Hall; 1997

[23] Christensen RM, Lo KH. Solutions for effective shear properties in three phase sphere and cylinder models. *Journal of the Mechanics and Physics of Solids*. 1979;**27**:315-330

[24] Barbero EJ. *Finite Element Analysis of Composite Materials Using Abaqus*. Boca Roca: CRC Press; 2013

[25] Soden PD, Hinton MJ, Kaddour AS. Lamina properties, lay-up configurations and loading conditions for a range of fiber-reinforced composite laminates. *Composites Science and Technology*. 1998;**58**:1011-1022

[26] Kaddour AS, Hinton JM. Input data for test cases used in benchmarking triaxial failure theories of composites. *Journal of Composite Materials*. 2012; **46**:2295-2312

[27] Kaddour AS et al. Mechanical properties and details of composite laminates for test cases used in the third world-wide failure exercise.

*Journal of Composite Materials*. 2013; **47**:2427-2442

[28] Segurado J, Llorca J. A numerical approximation to the elastic properties of sphere-reinforced composites. *Journal of the Mechanics and Physics of Solids*. 2002;**50**(10):2107-2121

[29] Melro AR, Camanho PP, Pinho ST. Generation of random distribution of fibres in long-fibre reinforced composites. *Composites Science and Technology*. 2008;**68**(9):2092-2102

[30] Chateau C, Gelebart L, Bornert M, Crépinc J. Micromechanical modeling of the elastic behavior of unidirectional CVI SiC/SiC composites. *International Journal of Solids and Structures*. 2015; **58**:322-334

[31] Gonzalez C, Llorca J. Mechanical behavior of unidirectional fiber-reinforced polymers under transverse compression: Microscopic mechanisms and modeling. *Composites Science and Technology*. 2007;**67**(13):2795-2806

[32] Jimenez FL, Pellegrino S. Constitutive modeling of fiber composites with a soft hyperelastic matrix. *International Journal of Solids and Structures*. 2012;**49**(3-4):635-647

[33] Huang Y, Jin KK, Ha SK. Effects of fiber arrangement on mechanical behavior of unidirectional composites. *Journal of Composite Materials*. 2008; **42**(18):1851-1871

[34] Cavalcante MAA, Pindera M-J, Khatam H. Finite-volume micromechanics of periodic materials: Past, present and future. *Composites, Part B*. 2012;**43**:2521-2543

[35] Aboudi J, Arnold SM, Bednarczyk BA. *Micromechanics of Composite Materials: A Generalized Multiscale Analysis Approach*. Oxford: Butterworth-Heinemann; 2012

- [36] Sertse HM, Goodsell J, Ritchey AJ, Pipes RB, Yu W. Challenge problems for the benchmarking of micromechanics analysis: Level I initial results. *Journal of Composite Materials*. 2018;**52**(1):61-80
- [37] Wang YC, Huang Z-M. A new approach to a bridging tensor. *Polymer Composites*. 2015;**36**(8):1417-1431
- [38] Sun CT, Vaidya RS. Prediction of composite properties from a representative volume element. *Composites Science and Technology*. 1996;**56**:171-179
- [39] Tsai JL, Chi YK. Investigating thermal residual stress effect on mechanical behaviors of fiber composites with different fiber arrays. *Composites, Part B*. 2008;**39**(4):714-721
- [40] DIGIMAT User Manual, Release 5.1.2, MSC Software Company; 2014
- [41] Benveniste Y, Dvorak GJ, Chen T. Stress fields in composites with coated inclusions. *Mechanics of Materials*. 1989; **7**:305-317
- [42] Hobbiebrunken T, Hojo M, Adachi T, Jong CD, Fiedler B. Evaluation of interfacial strength in CF/epoxies using FEM and in-situ experiments. *Composites, Part A*. 2006;**37**(12): 2248-2256
- [43] Mortell DJ, Tanner DA, McCarthy CT. In-situ SEM study of transverse cracking and delamination in laminated composite materials. *Composites Science and Technology*. 2014;**105**:118-126
- [44] Koyanagi J, Ogihara S, Nakatani H, Okabe T, Yoneyama S. Mechanical properties of fiber/matrix interface in polymer matrix composites. *Advanced Composite Materials*. 2014;**23**(5-6): 551-570
- [45] Budiansky B, Fleck NA. Compressive failure of fiber composites. *Journal of the Mechanics and Physics of Solids*. 1993;**41**:183-211
- [46] Kyriakides S, Arseculeratne R, Perry EJ, Liechti KM. On the compressive failure of fiber reinforced composites. *International Journal of Solids and Structures*. 1995;**32**:689-738
- [47] Basu S, Waas AM, Ambur DR. Compressive failure of fiber composites under multi-axial loading. *Journal of the Mechanics and Physics of Solids*. 2006; **54**:611-634
- [48] Zhou Y, Huang Z-M. Composite failure under longitudinal compression. Submitted for publication
- [49] París F, Correa E, Cañas J. Micromechanical view of failure of the matrix in fibrous composite materials. *Composites Science and Technology*. 2003;**63**(7):1041-1052
- [50] Wisnom MR. Factors affecting the transverse tensile strength of unidirectional continuous silicon carbide fibre reinforced 6061 aluminum. *Journal of Composite Materials*. 1990;**24**(7):707-726
- [51] Aboudi J. Micromechanical analysis of the strength of unidirectional fiber composites. *Composites Science and Technology*. 1988;**33**(2):79-96
- [52] Mayes S, Andrew C, Hansen J. Multicontinuum failure analysis of composite structural laminates. *Mechanics of Composite Materials and Structures*. 2001;**8**(4):249-262
- [53] Pindera MJ, Gurdal Z, Hidde JS, Herakovich CT. Mechanical and Thermal Characterization of Unidirectional Aramid/Epoxy, CCMS-86-08, VPI-86-29. Virginia Polytechnic Institute and State University; 1986
- [54] Wang YC, Huang Z-M. Bridging tensor with an imperfect interface. *European Journal of Mechanics - A/Solids*. 2016;**56**:73-91